On the Distinct Nature of Tropical Cyclone Convergence Zones that Induce Core Reformation

David A. Schecter[1*]

[1]*NorthWest Research Associates, Boulder, Colorado, USA*

Submitted to *Journal of the Atmospheric Sciences* October 4, 2024; accepted July 11, 2025

*Corresponding author address: NorthWest Research Associates, 3380 Mitchell Lane, Boulder, CO, USA, 80301. E-mail: schecter@nwra.com

ABSTRACT: Relatively weak tropical cyclones exposed to appreciable environmental vertical wind shear commonly possess localized off-center regions of prominent convective activity coinciding with enhanced low-level convergence. Under special circumstances, a subvortex can rapidly strengthen within this convergence zone (CZ) and become the kernel of a new inner core of the tropical cyclone. A previously proposed condition for such *core reformation* is revised to be less restrictive. With minimal ancillary assumptions, the revised condition is simply that τ_e should exceed τ_{cr}. Here, τ_{cr} is the time scale of core reformation neglecting the disruptive impact of vorticity expulsion from the CZ by the nondivergent background flow, and τ_e is the time scale for fluid parcels to horizontally escape the CZ. Semi-analytical and analytical formulas are provided for estimating τ_{cr} and τ_e, respectively. The revised condition is tested against several cloud-resolving simulations of strongly misaligned tropical cyclones. Essentially consistent with theoretical expectations, downtilt CZs are found to induce core reformation only after maintaining τ_e near or well above τ_{cr} for a time scale comparable to the latter (hours). In a detailed illustration of the dynamics associated with the opposite condition of τ_e falling well below τ_{cr}, locally amplified vorticity anomalies readily leave the CZ, and the negative eddy-flux of vorticity is large enough to prevent major CZ spinup.

1. Introduction

Relatively weak tropical cyclones exposed to appreciable environmental vertical wind shear commonly possess prominent regions of convection localized downshear or downtilt of the surface vortex center. This concentrated convection has the potential to abruptly generate a subvortex of sufficient strength to become the kernel of a new inner core of the tropical cyclone. Such an event is referred to herein as *core reformation*. This paper will derive a basic condition for the occurrence of core reformation and demonstrate its general consistency with several cloud resolving tropical cyclone simulations.

Despite observational limitations, there are well-documented cases of natural tropical cyclones appearing to exhibit some form of core reformation (Molinari et al. 2004,2006; Molinari and Vollaro 2010a; Rogers et al. 2020; Alvey et al. 2022; Stone et al. 2023). Various full-physics simulations have displayed analogous core reformation events and have presented more detailed pictures of the underlying thermo-fluid dynamics (Davis et al. 2008; Nguyen and Molinari 2015; Chen et al. 2018). Of central interest to most of the aforementioned studies is the role of core reformation in the intensification of a tropical cyclone exposed to moderate shear. One might reasonably infer from the pertinent literature that core reformation can help prevent weakening or facilitate an episode of intensification through the associated vertical alignment and reduced distance of convective forcing from the circulation center. In some cases, the reformation is seen as essential to the initiation of rapid intensification. In relation to this point, core reformation appears to initiate the archetypal "sprint mode" of rapid intensification described by Judt et al. (2023).

Rivera-Torres et al. (2023) recently attempted to identify the distinctive characteristics of a tropical cyclone near the time of core reformation— referred to therein as "downshear reformation".[1] Reformation events in the North Atlantic (between 1998 and 2020) were subjectively identified from archived National Hurricane Center discussions. Tropical cyclones supposedly experiencing core reformation were compared to others that were not despite having similar intensities and selected environmental parameters. The reformation events predominantly occurred in tropical

[1]Rivera-Torres and coauthors (2023) define downshear reformation as "the process where a new low-level center develops within asymmetric convection downshear, replacing the parent vortex." Apart from the restriction to downshear locations, this definition appears to be consistent with the present concept of core reformation.

storms exposed to moderate deep-layer shear. Pertinent tropical cyclone fields were primarily extracted from ECMWF Reanalysis data (ERA5). The authors concluded the following:

> A comparison of storm-centered, shear-relative composite fields revealed several factors that differ between reformation and non-reformation cases. The reformed storms were characterized by:
>
> (i) An asymmetric distribution of mid- to upper-tropospheric relative humidity with higher values downshear and lower values upshear.
>
> (ii) Greater low-level relative humidity over much of the inner 500 km.
>
> (iii) Larger CAPE and low-level θ_e (equivalent potential temperature) right of shear.
>
> (iv) Larger surface latent heat fluxes left of shear and downshear due to stronger winds, associated with a stronger pressure gradient left of shear.

The present study does not attempt to challenge or thoroughly corroborate the foregoing conclusions on the moist-thermodynamic conditions supporting core reformation. Instead, this paper will aim to clarify a complementary condition on the kinematic properties of the tropical cyclone.

The focus will be on the localized convergence zone (CZ) at the base of a core reformation event. Schecter (2020; henceforth S20) proposed that core reformation will occur if a drifting CZ has sufficiently strong convergence to create an internal "point of attraction" that prevents entering fluid from horizontally escaping as its vorticity continually amplifies. An analytical expression for this "supercriticality" condition was derived and computationally verified (see also Schecter 2023). Because the issue was not of central importance to the article, S20 did not thoroughly examine the possibility of core reformation with weaker (subcritical) levels of convergence. This paper will address the preceding deficiency by revisiting basic CZ dynamics and deriving a semi-analytical condition for core reformation that does not rely on supercriticality. As noted earlier, the revised condition will be shown to have merit upon comparison to cloud resolving tropical cyclone simulations.

Before discussing theoretical and computational results, it is worthwhile to briefly disambiguate the definition of core reformation adopted for this study. The main problem is how to objectively determine when a core reformation event has occurred. While not necessarily identical to the requirements used elsewhere, the following criteria are used herein. First, the maximum azimuthally averaged tangential velocity of a subvortex developing in the area of a CZ must become stronger than that of the original inner core. Upon this achievement, the center ($\mathbf{x}_{cl}$ of section 3b) and characteristic radius (radius of maximum wind speed) of the inner core will have become those of the subvortex.

To provisionally qualify as a core reformation event, the coinciding transitions appearing in the time series of the center-coordinates and characteristic radius must occur *abruptly*, i.e., over a time scale much less than that of advection (cf. Fig. 4a of section 4). Furthermore, the new radius of the inner core must be appreciably smaller than the larger of the original radius or the distance between the new and original centers. Finally, the new inner core must remain convectively active so as not to readily (within hours) dissipate and lose its wind speed dominance to the broader circulation.

The remainder of this paper is organized as follows. Section 2 presents the revised theoretical condition for CZs to induce core reformation. Section 3 describes the configuration of the cloud resolving model used herein to simulate tropical cyclones, and explains various techniques used to analyze the output. Sections 4-6 demonstrate that the newly proposed condition for core reformation is generally consistent with the success or failure of CZs to produce new inner cores in several tropical cyclone simulations. Section 7 summarizes the main conclusions. Appendices A and B contain supplemental analyses, and appendix C contains reference tables for various symbols that are used throughout the manuscript.

2. Basic Theoretical Considerations

The present strategy for deriving a testable condition for core reformation involves breaking the problem into two simplified parts. The first part (section 2a) considers a CZ placed at the center of a broader axisymmetric vortex representing the bottom layer of a tropical cyclone. An analytical solution is readily obtained for the strengthening velocity field. The aforementioned solution is used to find the time at which the maximum wind speed of a subvortex spinning up within the CZ first exceeds that of the broader vortex. The time scale required for the subvortex to achieve supremacy is interpreted as the natural (unimpeded) time scale of core reformation for a given absolute vorticity[2] profile surrounding the CZ. The second part (section 2b) considers a CZ shifted outward to where background winds can act to expel convergence-enhanced vorticity and thus counteract the reformation effort. An analytical estimate for the characteristic time scale of vorticity expulsion (the escape time) is derived. Contingent on minimal secondary criteria, it is proposed that core reformation will occur if (and only if) its natural time scale stays shorter than the escape time. The detailed argument is given below.

[2]Unless stated otherwise, "vorticity" refers to vertical vorticity.

2a. Simple Model of Axisymmetric Core-Reformation

Consider a conceptual model in which the bottom layer of a weak tropical cyclone is represented by an axisymmetric vortex on the f-plane with a circular CZ of radius r_σ (wherein convection implicitly occurs) provisionally located on center. Suppose that the initial relative vorticity distribution of the cyclone has the form

$$\zeta_o(r) = 2\Omega_o \left[H(r_m - r) + \varepsilon \frac{r_m}{r_\sigma} H(r_\sigma - r) \right], \tag{1}$$

in which r is the radial coordinate, $0 \leq \varepsilon < 1$, and $H(x) = 1$ (0) if x is greater than (less than) zero. The preceding distribution has one component of uniform intensity $2\Omega_o$ extending to $r_m > r_\sigma$, and another component permitting a limited initial enhancement of vorticity (proportional to ε) within the CZ. The associated initial azimuthal velocity field (v) is given by

$$v_o(r) = \Omega_o r_m \left[\frac{\min(r, r_m)}{\max(r, r_m)} + \varepsilon \frac{\min(r, r_\sigma)}{\max(r, r_\sigma)} \right]. \tag{2}$$

For simplicity, let us further suppose that the convergence distribution has a constant positive value of σ inside the CZ and is zero outside, so that the radial velocity field (u) is given by

$$u_\sigma(r) = -\frac{\sigma r_\sigma}{2} \frac{\min(r, r_\sigma)}{\max(r, r_\sigma)}. \tag{3}$$

It should be noted in passing that r_m and r_σ respectively correspond to the initial radii of maximum azimuthal and radial wind speeds.

Over time, a secondary maximum of azimuthal velocity may emerge in the CZ and then dominate the outer maximum belonging to the broader cyclone. This process constitutes a special axisymmetric version of core reformation. The following calculates the time at which the secondary maximum becomes larger than its outer counterpart. Frictional damping will be neglected. The appropriateness of such neglect for understanding core reformation is addressed in appendix A.

The first step is to find a solution for the time-dependent azimuthal velocity field $v(r,t)$. Conservation of the absolute angular momentum of fluid parcels (rings) converging toward the center of the cyclone requires that

$$v(r,t) = \frac{r_o}{r} v_o(r_o) + \frac{f}{2r}(r_o^2 - r^2), \tag{4}$$

in which $r_o(r,t)$ is the initial radius of the parcel located at r when the time is given by t. The initial radius satisfies the equation $\partial r_o / \partial t = -u_\sigma(r_o)$ with the boundary condition $r_o(r,0) = r$. The solution can be expressed as follows:

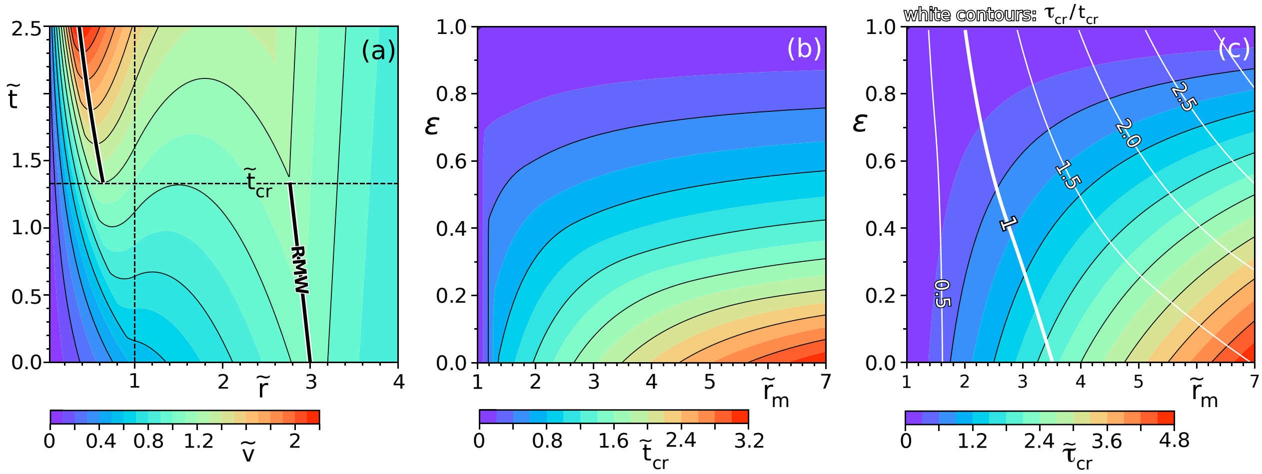

FIG. 1: (a) Illustrative evolution of the (normalized) azimuthal-velocity profile $\tilde{v}$ of an initially broad cyclone with a central CZ. Core reformation occurs at the time $\tilde{t}_{cr}$ when the radius of maximum wind speed (thick black curve) discontinuously jumps to a location inside the CZ ($\tilde{r} < 1$). Thin solid $\tilde{v}$-contours are spaced 0.2 units apart. System parameters are $\varepsilon = 0.2$, $\tilde{r}_m = 3$ and Ro = 4. (b) Variation of the normalized core reformation time $\tilde{t}_{cr}$ with ε and $\tilde{r}_m$ assuming Ro = 4. (c) As in (b) but for (color and black contours) the normalized time $\tilde{\tau}_{cr}$ ($\equiv \sigma\tau_{cr}$) required for intensification of the edge-velocity of the CZ to v_{mo}, and (white contours) the ratio of τ_{cr} to t_{cr}.

$$r_o^2 = \begin{cases} r^2 e^{\sigma t} & r < r_\sigma e^{-\sigma t/2}, \\ r_\sigma^2\left[1 + \sigma t - 2\ln(r_\sigma/r)\right] & r_\sigma e^{-\sigma t/2} \le r < r_\sigma, \\ r^2 + \sigma t r_\sigma^2 & r \ge r_\sigma. \end{cases} \tag{5}$$

Substituting Eqs. (2) and (5) into the right-hand side of Eq. (4) yields an analytical expression for v as a function of r and t from which the results of the next paragraph are derived.

Figure 1a shows the normalized azimuthal velocity field $\tilde{v} \equiv v/\Omega_o r_m$ as a function of the normalized coordinates $\tilde{r} = r/r_\sigma$ and $\tilde{t} \equiv \sigma t$, for a system with $\varepsilon = 0.2$, a scale ratio $\tilde{r}_m \equiv r_m/r_\sigma$ equal to 3, and an initial Rossby number Ro $\equiv 2\Omega_o/f$ equal to 4. In time, two distinct velocity peaks are clearly apparent. It is readily shown that the outer peak occurs at the radius $\tilde{r}_{out} = (\tilde{r}_m^2 - \tilde{t})^{1/2}$. The inner peak occurs at $\tilde{r}_{in} < 1$, which satisfies the transcendental equation $2\ln(\tilde{r}_{in}) + \tilde{r}_{in}^2/(1 + \text{Ro}) = 1 - \varepsilon\tilde{r}_m\text{Ro}/(1 + \text{Ro}) - \tilde{t}$. Core reformation occurs at the time $\tilde{t}_{cr}$ when the velocity of the inner peak grows to equal that of the outer peak. In other words, the core reformation time solves the equation $\tilde{v}(\tilde{r}_{in}, \tilde{t}_{cr}) = \tilde{v}(\tilde{r}_{out}, \tilde{t}_{cr})$. Figure 1b illustrates the solution in ε-$\tilde{r}_m$ parameter space for systems with Ro = 4.

A simpler estimate for the time scale of core reformation that will be used going forward is given by the time τ_{cr} required for the azimuthal velocity at the edge of the CZ to equal the initial maximum represented by $v_{mo} \equiv v_o(r_m)$. Using Eqs. (4) and (5), the condition $v(r_\sigma, \tau_{cr}) = v_{mo}$ takes the form

$$\sqrt{1+\sigma\tau_{cr}}\, v_o(r_\sigma\sqrt{1+\sigma\tau_{cr}}) + \frac{f r_\sigma}{2}\sigma\tau_{cr} = v_{mo}. \tag{6}$$

Combining Eqs. (2) and (3) with Eq. (6) yields

$$\tau_{cr} = \frac{v_{mo} - v_o(r_\sigma)}{-u_\sigma(r_\sigma)} \frac{1}{2\Omega_o + f} \tag{7}$$

for the vortex at hand. Figure 1c illustrates the solution for τ_{cr} given by Eq. (7), and shows that its ratio to t_{cr} ($\equiv \tilde{t}_{cr}/\sigma$) roughly falls between 0.5 and 2.0 for pertinent values of $\tilde{r}_m$ between 1.6 and 4. The moderate difference between τ_{cr} and t_{cr} does not overtly imply that the former is less useful. The opposite may well be true. Internal dynamics within a realistic CZ could involve efficient vorticity mixing that tempers amplification of the inner azimuthal velocity peak and brings the time required to accomplish core reformation closer to τ_{cr} than t_{cr} when the latter is relatively short. Furthermore, t_{cr} is sensitive to the assumed radial distribution of convergence inside the CZ, whereas τ_{cr} is not (with σ interpreted as the CZ-mean convergence).

It is worth remarking that Eq. (6) can be rewritten as follows:

$$\int_{r_\sigma}^{r_\sigma\sqrt{1+\sigma\tau_{cr}}} dr\, r\, \eta_o(r) = r_\sigma[v_{mo} - v_o(r_\sigma)], \tag{8}$$

in which $\eta_o \equiv r^{-1}d[rv_o(r)]/dr + f$ represents the initial distribution of absolute vorticity. The rate at which the left-hand side of Eq. (8) increases with $\sigma\tau_{cr}$ clearly increases with the magnitude of η_o beyond r_σ. It follows that $\sigma\tau_{cr}$ shortens not only with increasing circulation on the periphery of the CZ $[v_o(r_\sigma)]$, but also with increasing absolute vorticity surrounding the CZ. This fairly general result is reflected in the particular solution for τ_{cr} [Eq. (7)] when v_o is given by Eq. (2).

2b. Hypothetical Condition for Core Reformation Induced by an Off-Center CZ

Next consider a system in which the uniform circular CZ is displaced a distance substantially greater than r_σ from the center of the broader cyclone whose velocity field is here denoted by $\mathbf{u}_{\text{cyc}}$. Suppose that the CZ is allowed to drift with a velocity $\mathbf{c}_\sigma$, which in a real system might be partially coupled to the motion of an overlapping midlevel vortex. Suppose further that there exists a synoptic scale (en-

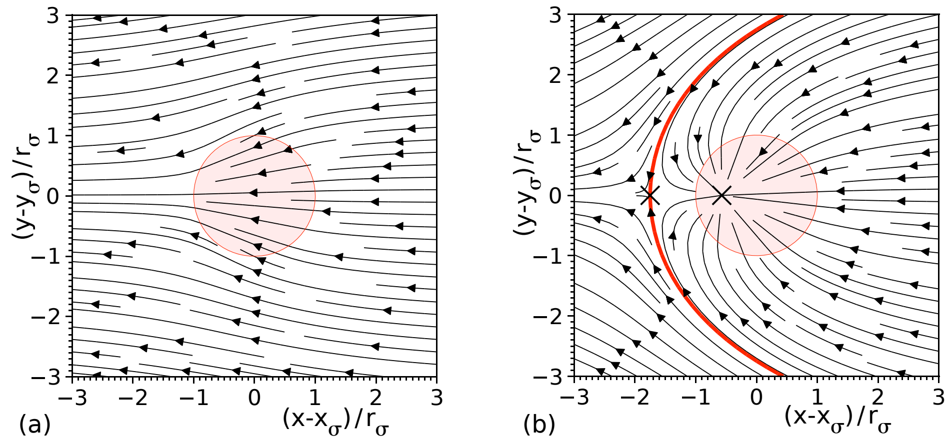

FIG. 2: Idealized off-center CZs (pink circles) with (a) subcritical and (b) supercritical intensities given by $\sigma = 0.5\sigma_c$ and $1.75\sigma_c$, respectively. Streamlines are shown in the CZ-relative reference frame and neglect the influence of local vorticity anomalies. Each $\times$ in (b) marks a stagnation point, and the thick red curve separates fluid that is destined to be trapped in the supercritical CZ from fluid that can pass by.

vironmental) velocity field $\mathbf{u}_{\rm env}$ superimposed over the cyclonic circulation and that potentially complex asymmetric vorticity perturbations in the vicinity of the CZ are initially negligible.

For the immediate purpose, the initial velocity field in a reference frame that moves with the center $\mathbf{x}_\sigma$ of the CZ can be approximated near and within the CZ by[3]

$$\mathbf{u}_o^* = \mathbf{U}_{\rm bg}^* + u_\sigma(\varrho)\hat{\boldsymbol{\varrho}}, \tag{9}$$

in which $\mathbf{U}_{\rm bg}^* \equiv \mathbf{u}_{\rm cyc}(\mathbf{x}_\sigma) + \mathbf{u}_{\rm env}(\mathbf{x}_\sigma) - \mathbf{c}_\sigma$ is the locally constant velocity of the background flow, u_σ is given by Eq. (3), and ϱ ($\hat{\boldsymbol{\varrho}}$) is the radius (radial unit vector) in a polar coordinate system centered on $\mathbf{x}_\sigma$. S20 demonstrates that the flow in Eq. (9) falls into one of two categories depending on whether σ is greater or smaller than the critical value

$$\sigma_c \equiv 2|\mathbf{U}_{\rm bg}^*|/r_\sigma. \tag{10}$$

Figures 2a and 2b respectively depict subcritical ($\sigma < \sigma_c$) and supercritical ($\sigma > \sigma_c$) conditions for cases in which $\mathbf{U}_{\rm bg}^*$ points westward (in the negative x-direction).

The streamlines in Fig. 2a suggest that fluid parcels undergoing vorticity enhancement (while horizontally contracting and losing mass through convection) within a subcritical CZ will eventually escape barring a radical change to the flow structure (cf. Fig. 12 of S20). The escape time can be estimated by the time required for a parcel to move from the center of the drifting CZ to

[3]Throughout this paper, horizontal velocities in the CZ-relative reference frame are generally indicated by an asterisk.

its outer edge under the imaginary scenario in which the CZ-relative flow remains steady. In the foregoing scenario, the parcel moves outward with the velocity $d\varrho_p/dt = |\mathbf{U}^*_{\mathrm{bg}}| + u_\sigma(\varrho_p)$ relative to the CZ center. Integrating the preceding velocity equation forward in time yields $\varrho_p = 2|\mathbf{U}^*_{\mathrm{bg}}|[1 - \exp(-\sigma t/2)]/\sigma$ while $0 \le \varrho_p \le r_\sigma$. The time at which $\varrho_p = r_\sigma$ is thus

$$\tau_e = -\frac{2}{\sigma}\ln\left(1 - \frac{\sigma}{\sigma_c}\right), \quad (11)$$

which grows from $r_\sigma/|\mathbf{U}^*_{\mathrm{bg}}|$ to ∞ as σ/σ_c grows from 0^+ to 1. The escape time clearly remains infinite for supercritical systems with larger ratios of σ to σ_c owing to the emergence of an attractive stagnation point (Fig. 2b).

The horizontal escape of fluid parcels from the CZ into the broader circulation is presumably detrimental to local vorticity buildup and the process of core reformation. One might therefore expect core reformation to be possible only if τ_e is appreciably longer than the time scale τ_{cr} for a subvortex in the CZ to intensify to the point of dominating the broader cyclone when background advection is neglected. Under common situations the preceding condition may also be sufficient.

The working estimate of τ_{cr} needed for comparison to τ_e will be obtained from a computational solution of Eq. (6), slightly reinterpreted to account for displacement of the CZ. Specifically, v_o will be viewed as the azimuthally averaged tangential velocity in a CZ-centered ($\mathbf{x}_\sigma$-centered) coordinate system, or equivalently one-half of ϱ times the mean relative vorticity inside of ϱ. The value of v_{mo} will still be set to the maximum azimuthally averaged tangential velocity in a coordinate system whose center ($\mathbf{x}_{cl}$ of section 3b) lies on that of the tropical cyclone. Note that the assumption built into Eq. (6) that u_σ decays as ϱ^{-1} out to $r_o^{cr} \equiv r_o(r_\sigma, \tau_{cr})$ appears to be adequate for the principal case studies analyzed herein (see appendix B).

One caveat of the foregoing discussion is that core reformation requires more than CZ spinup. A reformation event should also involve an abrupt (virtually discontinuous) change from the original to new inner core. Such an abrupt change would seem to prohibit the CZ from entraining most of the original inner core during spinup of the subvortex prior to the reformation time. One might intuitively interpret this to mean that r_o^{cr} should be appreciably smaller than the lengthscale λ representing the larger of the (original) radius of maximum wind speed or distance between the CZ and the center of the inner core. It is presently conceivable to the author that violations of this criterion could exist for some off-center CZs.

In summary, it seems reasonable to hypothesize that core reformation should occur in a tropical cyclone *iff* the following conditions are met. Of primary importance for enabling CZ spinup, the kinematic state should satisfy

$$\tau_{cr} < \tau_e, \tag{12}$$

in which τ_e is estimated from Eq. (11) and τ_{cr} from Eq. (6) as explained two paragraphs above. On intuitive grounds, an abrupt change of the inner core would also seem to require that $r_o^{cr} < \lambda$, which amounts to $\tau_{cr} < [(\lambda/r_\sigma)^2 - 1]/\sigma \equiv \tau_\lambda$ given approximate ϱ^{-1} decay of outer u_σ. Bear in mind that the preceding conditions must persist over the time τ_{cr} required for the strengthening subvortex within the CZ to achieve dominance over the broader cyclone. Prediction of such persistence in a tropical cyclone would require a supplemental theory for the duration and propagation of the convection associated with the CZ. Such a predictive theory based on local meteorological conditions is beyond the scope of this paper. The present investigation is limited to an initial test of whether sufficiently long maintenance of condition (12) in conjunction with the abruptness criterion truly distinguishes CZs that successfully induce core reformation from those that do not in quasi-realistic simulations.

2c. Some Complications

The foregoing theoretical considerations ignored some details of the eddy-flux of vorticity at the boundary of the CZ that could be relevant to a realistic system. One might imagine (for example) that positive vorticity anomalies in the inflowing airstream could add an eddy-flux that acts to accelerate CZ spinup and thus reduce the minimum magnitude of τ_e required for core reformation. The potential importance of positive contributions to the net eddy-flux will not be thoroughly assessed herein, but will be addressed to some extent in section 4c.

The preceding considerations also neglected the fine structure of a CZ (related to the intricacies of natural convection) that may have some bearing on whether core reformation will occur. Such fine structure could entail pockets of intense convergence (or divergence) anomalies within the larger convergence field of mean intensity σ. Pockets of intense convergence moving along with the local background flow might rapidly generate proportionally small but strong subvortices. One such convergence anomaly could conceivably initiate core reformation on a smaller scale than that of the CZ, even when a smoothed representation of the CZ fails to satisfy condition (12). That being said, a more probable scenario may involve fine scale convergence anomalies that are too short-lived or otherwise unable to spin up a new and robust inner core without collective action.

Despite exceptions that may arise due to fine scale dynamics, we will proceed assuming that core reformation occurs (if at all) on the lengthscale r_σ determined to adequately measure the full extent of the CZ. Consistently, we will continue to assume that the time scale for unimpeded core reformation is adequately obtained from Eq. (6) with σ representing the CZ-mean convergence. The general appropriateness of using Eq. (11) to estimate the escape time τ_e seems more questionable, because the pathways of parcel escape from the full CZ could still be sensitive to neglected structural details. The following describes two provisional methods that will be used to help evaluate the appropriateness of Eq. (11) for the CZs that appear in our simulated tropical cyclones.

The first method begins by approximating the low-level horizontal velocity field in the CZ-moving reference frame ($\mathbf{u}_l^*$) with a filtered version ($\mathbf{u}_f^*$) that keeps convergence anomalies of all scales within the CZ but eliminates vorticity anomalies at scales smaller than the broader cyclonic circulation. A probability distribution $\mathcal{P}_f(\tau_e)$ is then computationally obtained for the time τ_e required for fluid parcels evenly spread within a radius r_σ from the CZ-center to escape the CZ along the streamlines of $\mathbf{u}_f^*$, in the artificial scenario where the velocity field is frozen in time. Comparison of this distribution to τ_e given by Eq. (11) will offer some quantitative insight into the adequacy of the latter.

The specific formula for the filtered velocity field is given by

$$\mathbf{u}_f^* \equiv \bar{v}_b(r)\hat{\boldsymbol{\varphi}} + \mathbf{u}_\chi + \mathbf{u}_a - \mathbf{c}_\sigma. \tag{13}$$

Here, $\bar{v}_b(r)$ is the azimuthal mean of the tangential velocity ($\mathbf{u}_l^* \cdot \hat{\boldsymbol{\varphi}}$) in a polar coordinate system (r, φ) whose origin lies on the center of the broader cyclone ($\mathbf{x}_{cl}^b$ of section 3b). The second component of $\mathbf{u}_f^*$ accounts for all features of the convergence field within the CZ. It is given by $\mathbf{u}_\chi \equiv \nabla_h \chi$, in which ∇_h is the horizontal gradient operator and

$$\nabla_h^2 \chi = \frac{\nabla_h \cdot \mathbf{u}_l^*}{2} \left\{ 1 + \cos\left[\pi \frac{\max(\,0,\, \min(\varrho - r_\sigma, \delta\varrho)\,)}{\delta\varrho} \right] \right\} + \delta\sigma. \tag{14}$$

The coefficient of $\nabla_h \cdot \mathbf{u}_l^*$ in Eq. (14) can be seen to maintain a value of unity as the radius ϱ from the center of the CZ increases from zero to r_σ, whereupon it attenuates to zero over a distance $\delta\varrho = 0.42 r_\sigma$. The Poisson equation for χ [Eq. (14)] is solved with periodic boundary conditions on the expansive domain used for the tropical cyclone simulations. Adding a very small constant

$\delta\sigma$ to the right-hand side is necessary to bring the horizontal domain average of the source field to zero. The final new variable appearing in the formula for $\mathbf{u}_f^*$ is $\mathbf{u}_a$, which represents the horizontal domain average of the velocity field in the (stationary) reference frame where the drift velocity $\mathbf{c}_\sigma$ of the CZ is measured.

The second method for assessing the potential impact of structural features neglected in deriving Eq. (11) considers a probability distribution $\mathcal{P}_u(\tau_e)$ for escape times along the unfiltered frozen streamlines of $\mathbf{u}_l^*$. The unfiltered velocity field incorporates contributions from all of the vorticity perturbations of the broader cyclonic distribution that were excluded from $\mathbf{u}_f^*$. While arguably having some advantages, this could also introduce new sources of error. For example, fluid parcels advecting out of the CZ within a sufficiently strong subvortex could deceptively seem trapped along quasi-circular orbits inside the CZ. Therefore, an uptick in the probability of infinite τ_e in switching from $\mathcal{P}_f$ to $\mathcal{P}_u$ may not indicate that the additional perturbations are enhancing the efficacy of vorticity buildup in the CZ. On the other hand, relatively small values of $\mathcal{P}_u(\tau_e)$ for all τ_e satisfying condition (12) could provide extra confidence that conditions are unsuitable for core reformation.

3. Essentials of the Cloud Resolving Simulations and Analysis Techniques

3a. Model Configuration

The tropical cyclone simulations considered in sections 4–6 of this study are from a data set generated by Cloud Model 1 (CM1; Bryan and Fritsch 2002) that is thoroughly described in Schecter (2024, henceforth S24). Each simulation is conducted on a doubly-periodic oceanic f-plane at 20 ^{o}N. The sea surface temperature (SST) is held constant in space and time but varies between simulations. The initial environmental vertical temperature and relative humidity distributions above the sea surface are taken from the Dunion (2011) moist tropical sounding.

The physics parameterizations are fairly conventional. Each simulation incorporates a variant of the two-moment Morrison cloud-microphysics module (Morrison et al. 2005,2009), having graupel as the large icy-hydrometeor category and a constant cloud-droplet concentration of 100 cm^{-3}. Radiative transfer is accounted for by the NASA-Goddard parameterization scheme (Chou and Suarez 1999; Chou et al. 2001). The influence of subgrid turbulence above the surface is accounted for by an anisotropic Smagorinsky-type closure analogous to that described by Bryan and Rotunno (2009). The horizontal mixing length l_h in each simulation increases linearly from

100 to 700 m as the surface pressure decreases from 1015 to 900 hPa. The asymptotic vertical mixing length l_v is 50 m. Surface fluxes are parameterized with bulk-aerodynamic formulas. The momentum exchange coefficient C_d increases from a minimum of 10^{-3} to a maximum of 0.0024 as the surface (10-m) wind speed increases from 5 to 25 m s^{-1} (compare with Fairall et al. 2003 and Curcic and Haus 2020). The enthalpy exchange coefficient is given by $C_e = 0.0012$ roughly based on the findings of Drennan et al. (2007). Heating associated with frictional dissipation is activated. Rayleigh damping is imposed above an altitude z of 25 km.

The equations of motion are discretized on a stretched rectangular grid that extends 2660 km in each horizontal dimension and 29.2 km in the vertical dimension. The 800×800 km^2 central region of the horizontal mesh (which contains the core of the tropical cyclone) has uniform increments of 2.5 km; the increments increase to 27.5 km at the four corners of the mesh. The vertical grid has 40 levels with spacing that gradually grows from 0.1 to 0.7 to 1.4 km as z increases from 0.05 to 8 to 29 km.

The simulations are initialized with the nominal pre-depression vortex shown in Fig. 1 of Schecter and Menelaou (2020). A domain-wide (environmental) zonal shear flow of variable intensity is introduced roughly two days into each simulation. The ground-relative winds change from easterly in the lower troposphere to westerly in the upper troposphere over a transition layer of depth $2\delta z_{\rm sh}$ centered at $z = z_{\rm sh}$. The values of $z_{\rm sh}$ and $\delta z_{\rm sh}$ are respectively 5.5 and 3.5 km (section 4) or 5.0 and 2.5 km (sections 5 and 6). Further details pertaining to the structure and maintenance of the shear flow can be found in S24.

3b. Center Finding Conventions

Forthcoming analyses of the cloud resolving simulations rely on reasonable definitions for the center $\mathbf{x}_{cl}$ of the low-level inner core of the tropical cyclone, the center $\mathbf{x}_{cl}^b$ of the broader (than CZ-scale) low-level cyclonic circulation, and the center $\mathbf{x}_{cu}$ of the midlevel (upper) vortex. The horizontal position vectors $\mathbf{x}_{cl}$ and $\mathbf{x}_{cl}^b$ are extracted from the horizontal velocity field vertically averaged over the 1-km deep boundary layer ($\mathbf{u}_l$). The location of $\mathbf{x}_{cl}$ is defined to be where a polar coordinate system (r, φ) must be centered to maximize the peak value of the azimuthal-mean tangential velocity profile $\bar{v}_l(r) \equiv \int_{-\pi}^{\pi} d\varphi(\mathbf{u}_l \cdot \hat{\varphi})/2\pi$ for $r \geq r_c$, in which $r_c = 10$ km. The location of $\mathbf{x}_{cl}^b$ is defined in a similar manner but with $r_c = r_c^b$, in which $r_c^b = 120$ km (except when reduced to

90 km for the analyses in Figs. 18d and 18e). Note that $\mathbf{x}_{cl}^{b}$ equals $\mathbf{x}_{cl}$ when the radius of maximum wind speed r_m of the low-level inner core equals or exceeds r_c^b. Such is generally the case prior to (but not in the hours after) the core reformation events considered herein. The definition of $\mathbf{x}_{cu}$ is similar to that of $\mathbf{x}_{cl}$, but with $\mathbf{u}_l$ replaced by the horizontal velocity field vertically averaged over a roughly 1-km thick layer centered just below $z = 8$ km.

The center of the low-level convergence zone $\mathbf{x}_\sigma$ is obtained from a two-step procedure. The first step finds a provisional center $\mathbf{x}'_\sigma$ where a polar coordinate system (ϱ, ϕ) must be centered to maximize the peak value of the azimuthal-mean radial inflow velocity $\bar{u}_l^-(\varrho) \equiv -\int_{-\pi}^{\pi} d\phi (\mathbf{u}_l \cdot \hat{\boldsymbol{\varrho}})/2\pi$ for $\varrho \geq \varrho_c$, in which $\varrho_c = 50$ km. The second step entails redefining the convergence center to be the centroid of enhanced convergence in the vicinity of $\mathbf{x}'_\sigma$. Specifically,

$$\mathbf{x}_\sigma \equiv \frac{\iint_A dA\, \mathbf{x}\, \sigma_l\, H(\sigma_l - \sigma_+)}{\iint_A dA\, \sigma_l\, H(\sigma_l - \sigma_+)}, \tag{15}$$

in which A denotes the area within a radius ϱ_A of $\mathbf{x}'_\sigma$, ϱ_A is the larger of 75 km and the radius of maximum $\bar{u}_l^-$, $\mathbf{x}$ is the horizontal position vector, $\sigma_l \equiv -\nabla_h \cdot \mathbf{u}_l$, and $\sigma_+ = 1.5 \times 10^{-3}$ s^{-1} is a convergence threshold. The location of $\mathbf{x}_\sigma$ defined by Eq. (15) can be noticeably closer than $\mathbf{x}'_\sigma$ to the strongest convergence anomaly within the CZ.

When required for analysis, the drift velocity $\mathbf{c}_\sigma(t)$ of the CZ is obtained (unless stated otherwise) from a least-square fit of $\mathbf{x}_\sigma(t')$ to the linear function $\mathbf{x}_\sigma^o + \mathbf{c}_\sigma t'$ over the time interval $[t'_-, t'_+]$, in which $t'_\pm = t \pm 15$ min. If sampling intervals of length δt (3 min) exist between t'_- and t'_+ over which the distance δx_σ between the initial and final CZ center exceeds the threshold $c_m \delta t$, then t'_- (t'_+) is increased (decreased) by the minimum amount until all such sampling intervals are excluded from the fit interval. The threshold coefficient c_m for the pre-hurricane systems analyzed herein is set to 75 m s^{-1}. It is commonly the case that when δx_σ exceeds its threshold, $\mathbf{x}_\sigma$ corresponds to distinct CZs on opposite ends of the sampling interval.

4. A Tropical Cyclone Simulation that Exhibits Core Reformation

4a. The Main Event

Figure 3 illustrates core reformation in a tropical cyclone simulation with an SST of 32 ^{o}C and an applied environmental vertical wind shear measuring 10.5 m s^{-1} between the surface and 12 km above

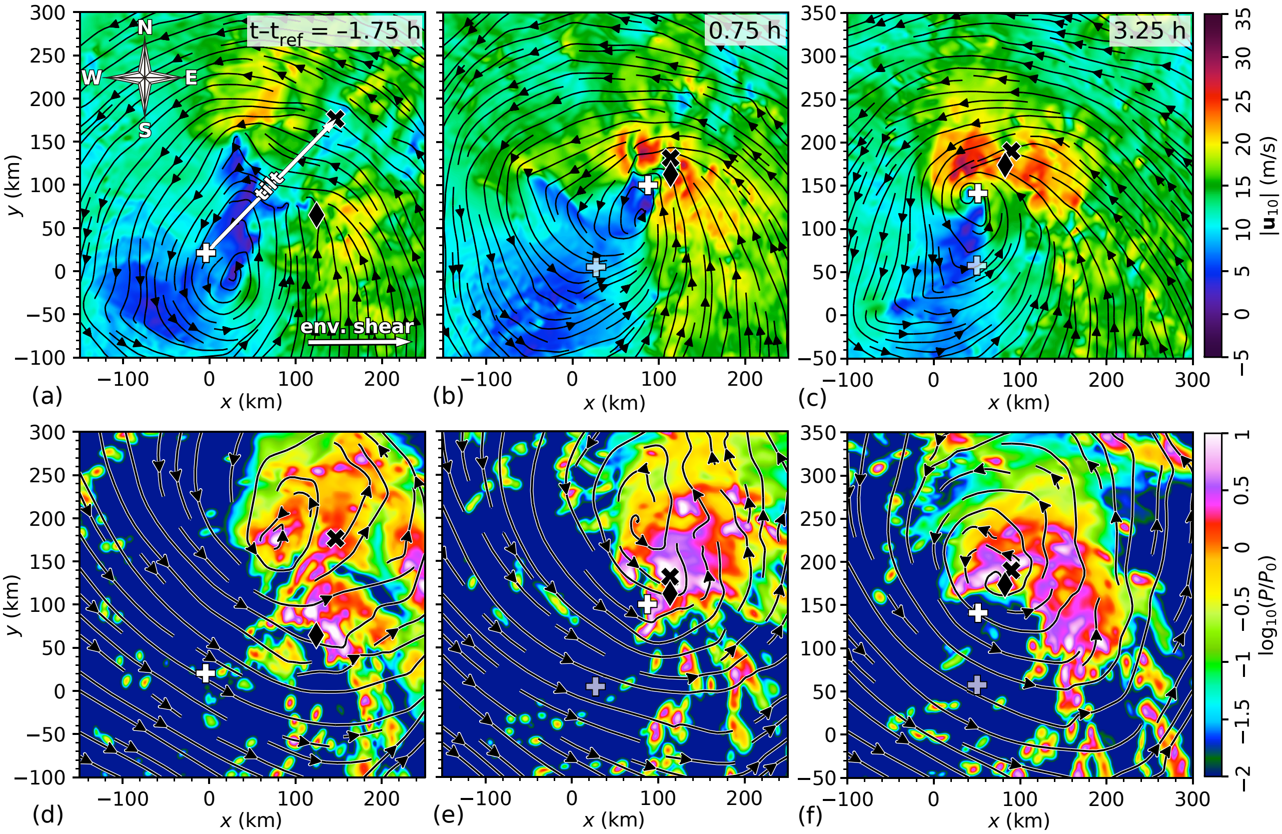

FIG. 3: (a-c) Snapshots of the streamlines and magnitude of the ground-relative velocity 10 m above the surface ($\mathbf{u}_{10}$) in a 5-h time frame surrounding core reformation in a tropical cyclone simulated with moderate environmental vertical wind shear over a warm ocean. Time measured from the official moment of reformation is shown on the top-right corner of each panel. Various symbols mark the locations of the low-level inner-core vortex center $\mathbf{x}_{cl}$ (opaque white +), the low-level broader cyclone center $\mathbf{x}^b_{cl}$ (semi-transparent white +), the midlevel vortex center $\mathbf{x}_{cu}$ (black ×) and the low-level convergence center $\mathbf{x}_\sigma$ (♦). Note that $\mathbf{x}_{cl} = \mathbf{x}^b_{cl}$ in (a). (d-f) As in (a-c) but for the midlevel ($z \approx 8$ km) streamlines superimposed over the base-10 logarithm of the 6-min surface precipitation rate P normalized to $P_0 = 1$ cm h^{-1}.

sea level. The top row shows snapshots of the magnitude and streamlines of the ground-relative surface velocity field 1.75 h before, 0.75 h after and 3.25 h after the time in the simulation when core reformation officially occurs (t_{ref}). The bottom row shows corresponding snapshots of the midlevel ($z = 7.8 \pm 0.7$ km) streamlines superimposed over the 6-min surface precipitation rate. A prominent CZ marked by the black diamond can be seen to develop in conjunction with strong convection and heavy precipitation slightly to the right of the tilt vector, roughly midway between the low-level and midlevel circulation centers (left column). Shortly thereafter, a subvortex extending from the surface to the upper part of the troposphere within the CZ becomes dominant, and thus replaces the initially larger inner core of the tropical cyclone (middle column). Although vertical wind shear and internal processes may continually adjust the size and alignment of the new core in the aftermath of reformation, the new core seems to remain a permanent fixture of the system.

Figure 4a shows various time series of tropical cyclone parameters during a 6-h period surrounding core reformation. The aforementioned parameters include the radius r_m at which $\bar{v}_l$ is maximized in the $\mathbf{x}_{cl}$-centered coordinate system, the tilt magnitude $|\mathbf{x}_{cu} - \mathbf{x}_{cl}|$, the distance between the low-level convergence and inner-core vortex centers given by $\ell \equiv |\mathbf{x}_\sigma - \mathbf{x}_{cl}|$, and the distance between the low-level convergence and broader cyclone centers given by $\ell_b \equiv |\mathbf{x}_\sigma - \mathbf{x}_{cl}^b|$. The core reformation event at $t_{\mathrm{ref}} = 103.75$ h is characterized by an abrupt reduction of tilt alongside major contractions of both r_m and ℓ. There is no coinciding discontinuity of ℓ_b, because the convergence and broader cyclone centers vary smoothly with time over the interval under consideration.

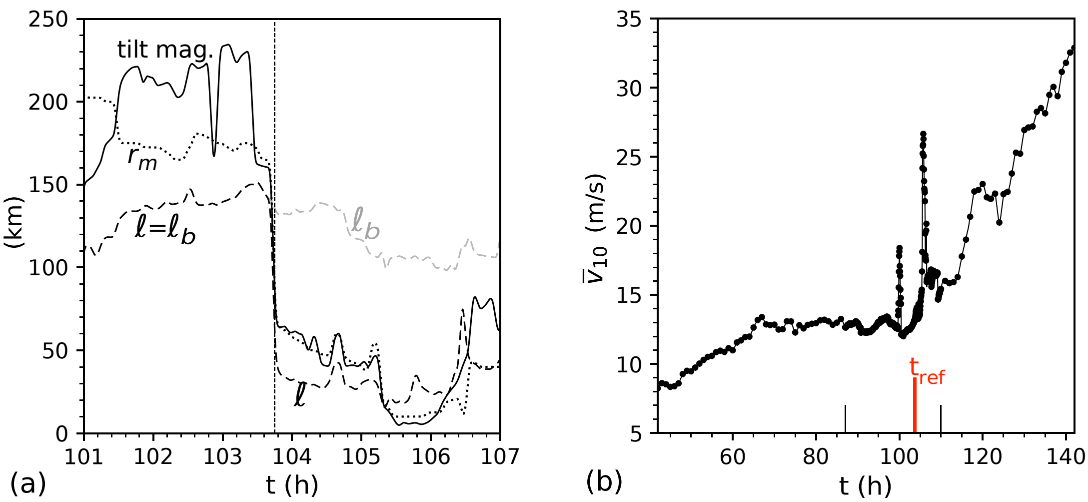

Fig. 4: (a) Time series of the tilt magnitude (solid curve) and low-level radius of maximum wind speed r_m (dotted curve). Distances of the convergence center from the inner-core vortex center (black dashed curve labeled ℓ) and from the broader cyclone center (gray dashed curve labeled ℓ_b) in the boundary layer are also shown. The time frame is limited to a 6-h period surrounding core reformation at $t_{\mathrm{ref}} = 103.75$ h. (b) Longer time series of the maximum azimuthally averaged tangential velocity of the tropical cyclone 10 m above the surface. The sampling interval between two consecutive dots is 3 min (1 h) in between (outside) the black ticks extending upward from the time axis.

Figure 4b shows a time series of the maximum azimuthally averaged tangential velocity $\bar{v}_{10}$ measured 10 m above the sea surface in the $\mathbf{x}_{cl}$-centered coordinate system. The core reformation event at t_{ref} is promptly followed by a sharp spike of tropical cyclone intensity corresponding to a transient collapse of r_m in the new core to roughly 10 km and a near elimination of tilt (Fig. 4a). Although the aforementioned spike is merely a fluctuation in the time series, the core reformation event apparently coincides with a transition to a longer trend of relatively fast intensification. The smaller spike preceding core reformation corresponds to a false (non-permanent) reformation event in a distinct downtilt convergence zone existing at the time. The residual effect of the subvortex created during the false event can be seen in Fig. 3a as a kink in the surface streamlines downwind of the tilt vector on the western edge of the main area of precipitation.

4b. Meteorological Conditions Immediately Preceding Core Reformation

Core reformation is generally observed to coincide with a vigorous and moderately long-lived convective subsystem within the broader tropical cyclone. Although not the focus of the present study, the following provides a brief description of the traditionally considered meteorological conditions supporting this convection.

Figure 5 shows snapshots of selected meteorological fields 15 minutes before the official reformation time. Figure 5a shows the distributions of CAPE (color) and CIN (contours) for 500-m "mixed layer" (ML) parcels assuming undiluted pseudoadiabatic ascent and liquid-only condensate. The computations of both variables follow the algorithm supplied in the CM1 software package. Here and elsewhere, the +, × and ⋄ respectively mark $\mathbf{x}_{cl}$, $\mathbf{x}_{cu}$ and $\mathbf{x}_{\sigma}$. The streamline directed into the convergence center corresponds to boundary layer flow in the CZ-relative reference frame ($\mathbf{u}_l^*$). Figure 5b shows the near-surface ($z = 50$ m) temperature distribution. The superimposed quiver plot shows the lower-tropospheric shear vector $\mathbf{S}_{\text{LT}} \equiv \mathbf{u}(z_\beta) - \mathbf{u}(z_\alpha)$, in which $z_\alpha = 0.05$ and $z_\beta = 2.67$ km. Figure 5c shows the lower-to-middle tropospheric relative humidity (RH) defined as the vertical average between $z = 2.3$ and 7.8 km. The RH is taken with respect to liquid (ice) condensate when the absolute temperature T is above (below) 273.15 K. The superimposed contours correspond to the 6-min surface precipitation rate. Figure 5d shows the bulk Richardson number shear defined by $\text{BSH} \equiv \frac{1}{2}(\mathbf{u}_{\text{bulk}} - \mathbf{u}_{\text{ML}})^2$, in which $\mathbf{u}_{\text{bulk}}$ ($\mathbf{u}_{\text{ML}}$) is the density weighted vertical average of the horizontal velocity $\mathbf{u}$ between the surface and $z = 6$ km (0.5 km). The contours shown mostly upstream of the CZ correspond to selected values of a rudimentary supercell composite parameter (SCP) based on Eq. (3) of Thompson et al. (2003) with unbounded components.[4] All plotted fields

[4]The value of MUCAPE applied to the SCP formula is estimated by the CAPE of the parcel deemed "most unstable" by virtue of having the greatest equivalent potential temperature in the lower troposphere. The nominal 0-3 km storm-relative helicity applied to the formula uses the estimate of Bunkers et al. (2000) for the velocity of right-moving storms; assuming right-movers is tenuously based on the tendency of lower-tropospheric shear vectors to turn clockwise with increasing z in the region where the SCP exceeds unity (Rotunno and Klemp 1982).

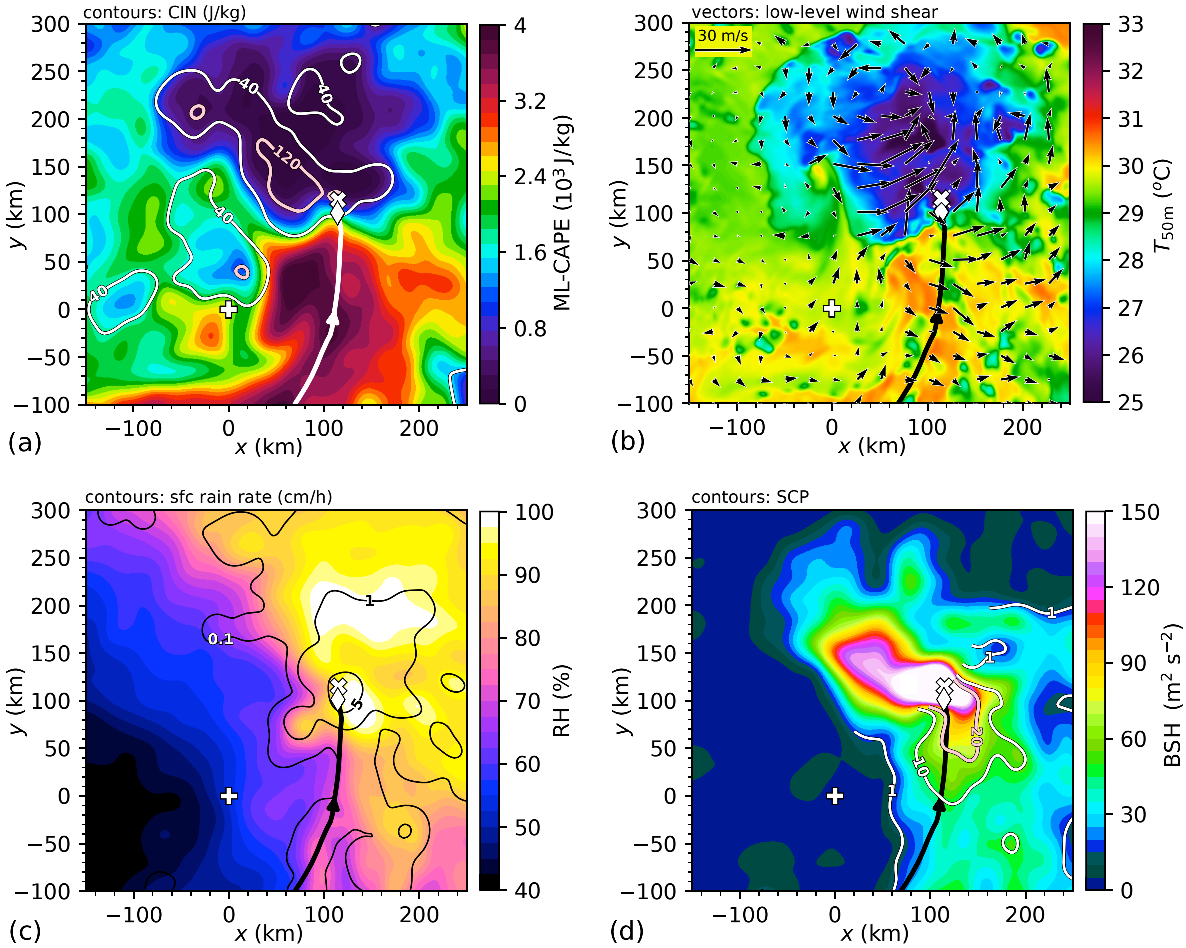

FIG. 5: Various fields pertinent to convection 15 minutes prior to the official time of core reformation (t_{ref}) in the tropical cyclone of Fig. 3. (a) Mixed layer CAPE (color) and CIN (contours). (b) Near-surface temperature (color) and low-level wind shear (vectors). (c) Lower-to-middle tropospheric relative humidity (color) and the 6-min surface precipitation rate (contours). (d) Bulk Richardson number shear (color) and the supercell composite parameter (contours). The thick CZ-relative streamline in each panel shows the instantaneous flow path into the convergence center. Distinct symbols mark the locations of $\mathbf{x}_{cl}$ (+), $\mathbf{x}_{cu}$ (×) and $\mathbf{x}_{\sigma}$ (◊).

excluding velocities and temperature are Gaussian smoothed with a standard deviation parameter of 10 km in both x and y so as to filter out meso-γ scale structure and facilitate viewing.

The boundary layer air mass streaming into the CZ where core reformation is imminent is seen to possess exceptionally high CAPE (Fig. 5a). While upstream CAPE exceeding 3000 J kg^{-1} may seem abnormal (cf. Molinari and Vollaro 2010b; Rivera-Torres et al. 2023), comparable values are not unheard of in real-world tropical disturbances (e.g. Smith and Montgomery 2012) and other tropical cyclone simulations illustrating rapid alignment or intensification (e.g. Alvey and Hazelton 2022; Judt et al. 2023). The area covering the CZ is seen to contain enhanced relative humidity above the boundary layer, which minimizes the potentially detrimental effects of

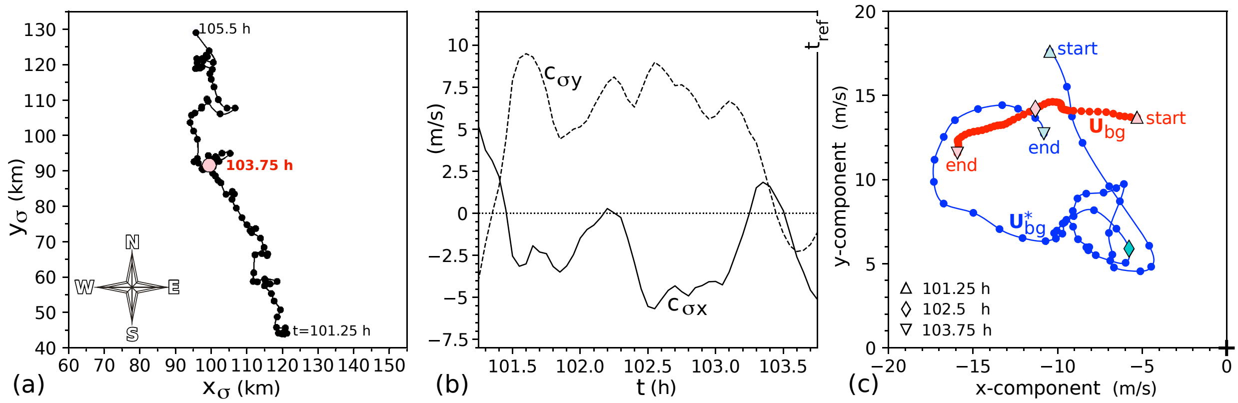

FIG. 6: (a) Trajectory of the convergence center $\mathbf{x}_\sigma$ during a time period surrounding core reformation, in a stationary coordinate system defined such that $\mathbf{x}^b_{cl} = (0,0)$ at $t_{\text{ref}} = 103.75$ h. The large pink circle marks $\mathbf{x}_\sigma$ at t_{ref}. (b) Time series of the x (solid) and y (dashed) components of the ground-relative drift velocity $\mathbf{c}_\sigma$ of the convergence center prior to t_{ref}. (c) Temporal hodographs of the local ground-relative ($\mathbf{U}_{\text{bg}}$, red) and CZ-relative ($\mathbf{U}^*_{\text{bg}}$, blue) background velocities at $\mathbf{x}_\sigma$ prior to t_{ref}.

entrainment on updrafts and facilitates intense deep convection, consistent with the presence of heavy precipitation (Fig. 5c). Note further that low humidity near the central and uptilt regions of the tropical cyclone may help confine vigorous deep convection to areas downtilt. Other reasons for such confinement have been discussed elsewhere (e.g., S24 and references therein) and will not be elaborated upon herein. The center of the CZ distinctly sits on the upstream edge of a prominent cold pool (Fig. 5b) that coincides with low CAPE and moderately high CIN (Fig. 5a). A substantial fraction of the cold pool is covered by rain falling at a rate above 1 cm h^{-1} (Fig. 5c). Low-level shear vectors roughly perpendicular to the velocity of the inflowing airstream (Fig. 5b) suggest that air entering the CZ has an appreciable level of streamwise vorticity that may be conducive to long-lasting highly rotational convection. Values of BSH and SCP respectively exceeding 40 m^2 s^{-2} and unity in the CAPE-enriched area upstream of the CZ (Fig. 5d) may also indicate conditions that are especially supportive of robust rotational convection, insofar as empirical results for midlatitude systems (Thompson et al. 2003) have relevance to convection in developing tropical cyclones (cf. Hendricks et al. 2004; Houze 2010; Kilroy and Smith 2015).

4c. Convergence Zone Dynamics in the Time Period of Core Reformation

Figure 6 illustrates the motion of the CZ and a theoretically important consequence of that motion. The data are limited to a time interval surrounding core reformation during which the CZ can be readily tracked. Figure 6a shows that the position of the CZ center $\mathbf{x}_\sigma$ gradually drifts northwestward with minor episodic deviations from its mean path. The corresponding ground-relative drift velocity

$\mathbf{c}_\sigma$ is plotted to the right (Fig. 6b) for $t \le t_{\mathrm{ref}}$. The red data in Fig. 6c show the temporal variation of the following spatially constant approximation of the ground-relative background velocity field within the CZ: $\mathbf{U}_{\mathrm{bg}} \equiv \mathbf{u}_{\mathrm{bg}}(\boldsymbol{\xi}_\sigma)$, in which

$$\mathbf{u}_{\mathrm{bg}}(\boldsymbol{\xi}) \;\equiv\; \bar{v}_b(|\boldsymbol{\xi}|)\,\hat{\mathbf{z}}\times\hat{\boldsymbol{\xi}} \;+\; \mathbf{u}_a. \tag{16}$$

Here, $\bar{v}_b$ is the azimuthally averaged tangential component of $\mathbf{u}_l$ about the broader cyclone center $\mathbf{x}_{cl}^b$, $\boldsymbol{\xi} \equiv \mathbf{x} - \mathbf{x}_{cl}^b$ ($\boldsymbol{\xi}_\sigma \equiv \mathbf{x}_\sigma - \mathbf{x}_{cl}^b$), $\hat{\boldsymbol{\xi}} \equiv \boldsymbol{\xi}/|\boldsymbol{\xi}|$, and $\mathbf{u}_a$ is the domain-average of $\mathbf{u}_l$. As in section 3b, $\mathbf{u}_l$ denotes the ground-relative z-averaged horizontal velocity field in the 1-km deep boundary layer. The blue data in Fig. 6c show the corresponding approximation of the background velocity field in the CZ-relative reference frame ($\mathbf{U}_{\mathrm{bg}}^* \equiv \mathbf{U}_{\mathrm{bg}} - \mathbf{c}_\sigma$) which varies in magnitude from 6.6 to 21.0 m s^{-1}. In theory, the extended period of diminished $|\mathbf{U}_{\mathrm{bg}}^*|$ near the blue diamond reduces the amount of convergence needed to effectively advance the process of core reformation (see section 2b).

Figure 7 depicts the evolution of various fields within the CZ during a 2.5-h visualization period ending at t_{ref}. The left column shows streamlines of the CZ-relative horizontal velocity field ($\mathbf{u}_l^* \equiv \mathbf{u}_l - \mathbf{c}_\sigma$) superimposed over the associated relative vorticity field $\zeta_l \equiv \hat{\mathbf{z}} \cdot \nabla_h \times \mathbf{u}_l$. The middle column shows streamlines of the filtered velocity field $\mathbf{u}_f^*$ of section 2c, which is essentially $\mathbf{u}_l^*$ minus contributions from all perturbations to the broader cyclonic vorticity distribution and all convergence anomalies outside of the dominant CZ. Here the streamlines are superimposed over the convergence field $\sigma_l \equiv -\nabla_h \cdot \mathbf{u}_l$. Without the irrotational flow attributed to convergence anomalies within the CZ, $\mathbf{u}_f^*$ would reduce to the CZ-relative background velocity field $\mathbf{u}_{\mathrm{bg}}^* \equiv \mathbf{u}_{\mathrm{bg}} - \mathbf{c}_\sigma$ [cf. Eq. (16)] that is shown to the right. The dashed gray circle in each panel is just large enough to contain virtually all of the most intense substructures of the convergence field (middle column) surrounding its center $\mathbf{x}_\sigma$ during the time period under consideration. The circle's 60-km radius is provisionally assumed to be that of the CZ denoted by r_σ, and is commensurate with the characteristic radius r_m of the new inner core of the tropical cyclone immediately after reformation (Fig. 4a). The green vector in each panel represents $\mathbf{U}_{\mathrm{bg}}^*$ (Fig. 6c) and notably tends to differ little from the purple vector representing the average of the velocity field associated with the streamlines inside the CZ.[5]

---

[5] To ease viewing, the vorticity and convergence fields in Figs. 7 and 15 are Gaussian smoothed with a standard deviation parameter of 2.5 km in both horizontal dimensions. Unsmoothed convergence fields generally have more regions peaking above the threshold value of $\sigma_+ = 1.5 \times 10^{-3}$ s^{-1} that is used to find $\mathbf{x}_\sigma$ (see section 3b).

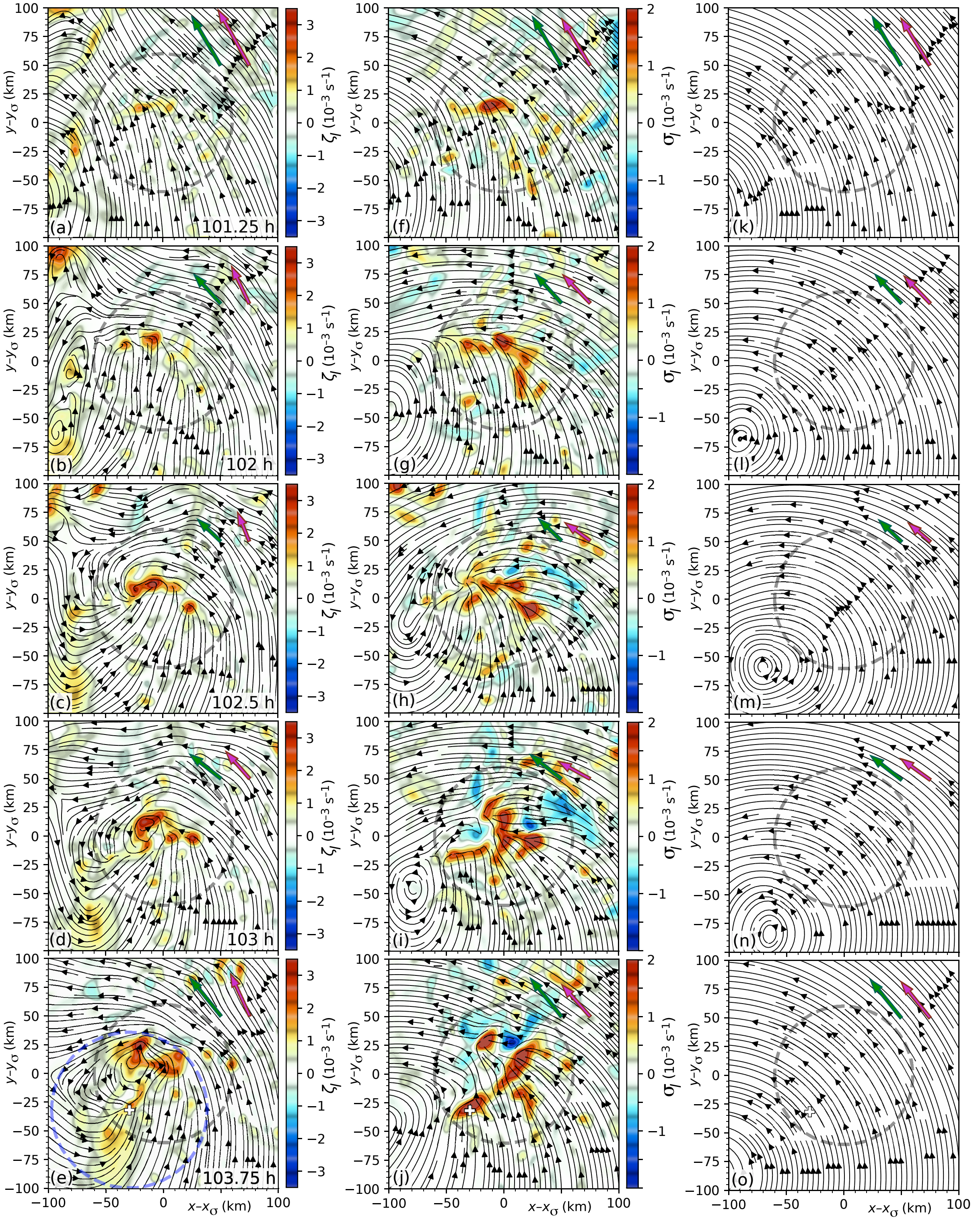

FIG. 7: (a-e) Snapshots of the boundary-layer relative vorticity field ζ_l (color) and streamlines of $\mathbf{u}_l^*$ during the 2.5 hours immediately preceding core reformation. (f-j) As in (a-e) but for the boundary-layer convergence field σ_l (color) and streamlines of the filtered velocity field $\mathbf{u}_f^*$. (k-o) Streamlines of the CZ-relative background velocity field $\mathbf{u}_{\rm bg}^*$. The purple vector in each panel shows the average of the velocity field depicted by the streamlines within a 60-km radius of $\mathbf{x}_\sigma$ (dashed gray circle), whereas the green vector shows $\mathbf{U}_{\rm bg}^*$. The length of the green vector in (a) corresponds to 20.1 m s^{-1}. The time printed in each left panel applies across the entire row. The white + entering the frame at $t_{\rm ref}$ = 103.75 h marks the objective location of $\mathbf{x}_{cl}$ at the instant of core reformation; the encompassing dashed blue circle in (e) has the radius r_m of the new inner core.

The amplification of an incipient vorticity perturbation into the kernel of a dominant subvortex centered within the CZ (left column) initially coincides with the growth of intense convergence anomalies (middle column) and reduction of the local CZ-relative background velocity. The streamlines of $\mathbf{u}_f^*$ (middle column) suggest that as the convergence anomalies mature alongside a diminishment of background advection, they occasionally (as at $t = 102.5$ h) show a strong capacity to horizontally trap local fluid parcels and thus efficiently amplify parcel vorticity. Without the maintenance of sufficiently strong convergence relative to the background flow, the latter (right column) would presumably eject the enhanced vorticity perturbation into the broader circulation before it could constitute the new core of the tropical cyclone.

Figure 8 shows the tangential velocity (circulation) budget along the periphery of the CZ for future comparison to a non-reformation scenario. The budget is constructed in a reference frame moving with the drift velocity $\mathbf{c}_\sigma$ of the CZ using a polar coordinate system (ϱ, ϕ) centered on $\mathbf{x}_\sigma$.[6] In this reference frame, the tendency of the azimuthally averaged tangential velocity v^* can be written as follows:

$$\frac{\partial \overline{v^*}}{\partial t} = -\overline{u^*}\overline{\eta} - \overline{u^{*\prime}\zeta^\prime} - \overline{w\frac{\partial v^*}{\partial z}} - \frac{c_{pd}}{\varrho}\overline{\theta^\prime_{\mathrm{den}}\frac{\partial \Pi^\prime}{\partial \phi}} + \overline{\mathcal{F}}_\phi, \tag{17}$$

in which $\eta \equiv \zeta + f$ is the absolute vorticity, $\zeta \equiv \hat{\mathbf{z}} \cdot \nabla_h \times \mathbf{u}^*$ is the relative vorticity, u^* (w) is the radial (vertical) velocity field, θ_{den} is the density potential temperature, Π is the Exner function, c_{pd} is the isobaric specific heat of dry air, and $\mathcal{F}_\phi$ is the azimuthal velocity forcing associated with parameterized turbulent momentum transport. In the present context, the overbar and prime respectively denote the azimuthal mean and perturbation (e.g., $u^{*\prime} = u^* - \overline{u^*}$) of a fluid variable. The contributions to the intensification rate of $\overline{v^*}$ on the right-hand side of Eq. (17) account for (from left to right) the influx of absolute vorticity driven by the mean flow, the eddy-influx of vorticity, vertical advection, the anticorrelation of $\theta^\prime_{\mathrm{den}}$ with the azimuthal pressure-gradient perturbation, and frictional torque largely attributable to surface drag. The plotted terms are vertical averages over the 1-km deep boundary layer evaluated at $\varrho = 60$ km (the provisional value of r_σ).

The time series in Fig. 8 suggest that the primary contributions to CZ spinup come from the horizontal influxes of planetary and relative vorticity via the mean flow (red) and eddies (blue).

[6]The algorithm used to compute the tangential velocity budget generally operates over 30-min intervals. During each sequential interval, $\mathbf{c}_\sigma$ is approximated by a constant value (instead of the sliding regression value used for all other types of analyses) and $\mathbf{x}_\sigma$ is approximated to have a linear trajectory.

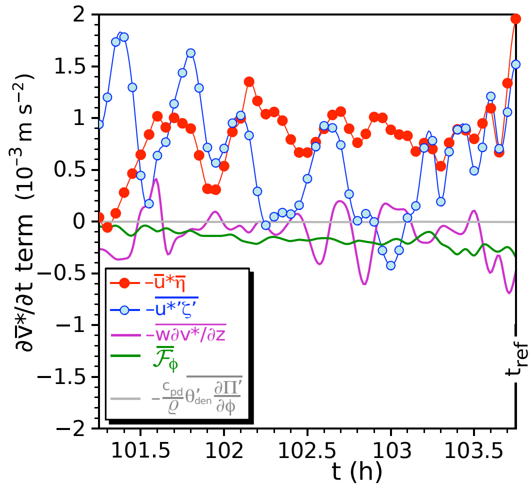

FIG. 8: Contributions to the azimuthal velocity tendency [right-hand side of Eq. (17)] along the periphery of the CZ in the hours preceding core reformation.

After a short growth period starting at the left-end of the plot ($t = 101.25$ h), the influx of η driven by the mean flow remains fairly steady, until jumping to an appreciably higher level moments before core reformation officially occurs ($t = t_{\text{ref}} = 103.75$ h). While less steady, the eddy-influx of vorticity prior to t_{ref} tends to be positive and thus cooperative on the whole toward enhancing the cyclonic circulation of the CZ. Substantial growth of the eddy-influx shortly before t_{ref} may well be connected to partial entrainment of a prominent vorticity anomaly at the edge of the southwest sector of the CZ (Fig. 7e). Bear in mind that the positive eddy-flux of vorticity seen here need not be essential to core reformation, so long as an alternative negative eddy-flux is subdominant to the positive influence of mean convergence on CZ spinup.

Moving forward, Fig. 9a shows the estimated time scale for fluid parcels to horizontally escape the CZ [τ_e given by Eq. (11)] normalized to the estimated time scale of unimpeded core reformation [τ_{cr} given by Eq. (6), interpreted as in section 2b with all variables extracted from $\mathbf{u}_l$] in the hours before t_{ref}.[7] Figures 9b and 9c show the coinciding time series of τ_{cr} and the strength σ of the CZ (the average of $-\nabla_h \cdot \mathbf{u}_l$ within a radius r_σ of $\mathbf{x}_\sigma$). As in the preceding CZ spinup analysis, the thick-solid curves are calculated with r_σ set to 60 km so as to approximately match the initial radius (r_m) of the reformed inner core. The broken curves are calculated with several other values

[7]Here and elsewhere (Figs. 11a, 17a, 18b and 18e), most of the variables in the referenced equations that give τ_e and τ_{cr} [$v_o(\rho)$, v_{mo} and σ] at a given time t are first averaged over the same 30-min (or smaller) interval about t used for the sliding linear regression that yields $\mathbf{c}_\sigma$ (see section 3b). The value of σ_c [in Eq. (11)] is evaluated with $\mathbf{U}^*_{\text{bg}}$ given by a similar sliding average of $\mathbf{U}_{\text{bg}}$ (defined as in Fig. 6c) minus the sliding regression result for $\mathbf{c}_\sigma$.

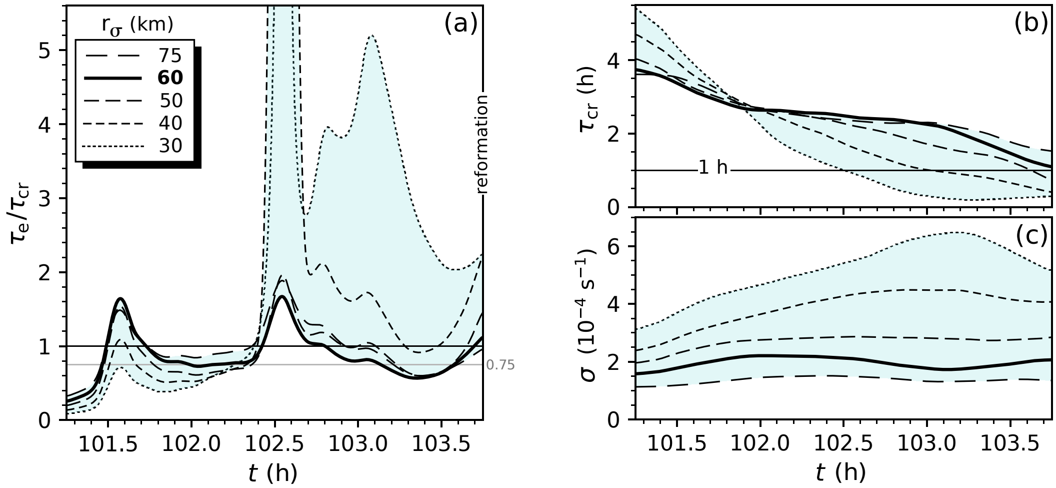

FIG. 9: (a) Estimated ratio of the escape time τ_e over the natural time scale of core reformation τ_{cr} in the hours before t_{ref}. The thick-solid curve assumes that the CZ-radius r_σ equals 60 km, so as to approximately match the initial half-width of the reformed inner core. The dashed and dotted curves show results for alternative values of r_σ (see legend). Light-cyan shading fills the space between the minimum and maximum values of τ_e/τ_{cr} obtained from the foregoing variation of r_σ. (b) As in (a) but for τ_{cr}. (c) As in (a) but for the mean convergence (σ) within a radius r_σ of $\mathbf{x}_\sigma$.

of r_σ (between 30 and 75 km) that span a range of conceivable alternatives gleaned from the middle column of Fig. 7.

First consider the results for $r_\sigma = 60$ km (solid curves). In the 2.5 hours before t_{ref}, the value of τ_{cr} monotonically decays from 3.8 to 1.1 h (Fig. 9b) in conjunction with gradual CZ spinup (Fig. 8) and modest net growth of σ (Fig. 9c).[8] Of particular note, the average value of τ_{cr} during this time period (2.4 h) is theoretically small enough for an unimpeded reformation process to complete. Section 2b proposed that τ_e should also exceed τ_{cr} to enable core reformation. In principle, the preceding condition renders the background flow ineffective in countering CZ spinup through its otherwise detrimental tendency to expel locally enhanced vorticity. Figure 9a shows that with r_σ set to 60 km, τ_e episodically exceeds but otherwise stays just under τ_{cr} in the immediate prelude of the reformation event. The latter feature suggests a modest discrepancy between the simulation and the hypothesized reformation condition. On the other hand, resetting r_σ to 40 or 30 km eliminates the discrepancy by raising τ_e/τ_{cr} above unity (Fig. 9a) over a 1.3-h time period that is no shorter than the coinciding reduced mean of τ_{cr} (Fig. 9b). The author cannot currently provide a definitive answer to why decreasing r_σ well below the initial radius of the reformed inner core robustly increases the

[8] The nonzero terminal value of τ_{cr} is sensible largely because of the unpredicted 43-km separation between $\mathbf{x}_{cl}$ and $\mathbf{x}_\sigma$ within the CZ (and a small difference between r_m and r_σ) that can be seen at $t = t_{\text{ref}}$ in Fig. 7.

ratio of τ_e to τ_{cr}, but he can offer a casual speculation. It may be that the vorticity buildup occurs more efficiently at a smaller lengthscale, but before triggering reformation on its own combines forces with external vorticity anomalies to create a new inner core of wider extent (Fig. 7e).

A similar reconciliation of the simulation results with the hypothesized reformation condition can be achieved while keeping r_σ at 60 km by accounting for structural details of the full CZ that were neglected in estimating the values of τ_e. Section 2c proposed considering two probability distributions for the escape times of parcels in two artificially frozen CZ-relative velocity fields. One probability distribution $[\mathcal{P}_u(\tau_e)]$ is for escape times in an unfiltered velocity field (left column of Fig.7), whereas the other $[\mathcal{P}_f(\tau_e)]$ is for escape times in a velocity field that accounts for the fine structure of the convergence field but filters out vorticity perturbations at all scales smaller than the broader cyclone (middle column of Fig. 7). Formally, both $\mathcal{P}_u$ and $\mathcal{P}_f$ denote probabilities per unit-τ_e. Figures 10a and 10b show the evolutions of the cumulative probability distributions defined by

$$C_{u/f}(\tau_e) \equiv \int_0^{\tau_e} d\tau_e' \, \mathcal{P}_{u/f}(\tau_e'). \quad (18)$$

Figure 10a demonstrates that after a brief transition period, the median τ_e (solid black curve) obtained from the unfiltered flow generally exceeds τ_{cr} (white curve) in the hours leading to core reformation. Moreover, there is an extended period just before the official moment of reformation ($102.4 < t < 103.2$ h) when over 75% of the parcels have $\tau_e \geq 8$ h $\gg \tau_{cr}$, and are thus effectively trapped in the artificial CZ (apart from mass lost through convection). Figure 10b shows similar results for the filtered flow. Whereas periods exist during which the median escape time along a filtered streamline is relatively small, it far more often exceeds τ_{cr}. Moreover, the filtering has minimal effect on the extended trapping period occurring shortly before t_{ref}. In summary, accounting for details of the CZ seems to fortify the conclusion that the process of core reformation coincides with conditions favoring prolonged retention and amplification of vorticity within the CZ.

Note that in addition to having probably (based on Fig. 10) underestimated τ_e for $r_\sigma = 60$ km in Fig. 9a, τ_{cr} may have been overestimated. This is because Eq. (6) ignores the positive eddy contribution to full-CZ spinup that exists for this particular system (Fig. 8). Given the moderate uncertainty in the time scale estimates, it may be best to view the hypothesized reformation condition to include a tacit coefficient μ close to unity, such that in reality it takes the form $\mu\tau_{cr} < \tau_e$. The specific value of μ that would minimize the failure rate of the foregoing condition in differentiating

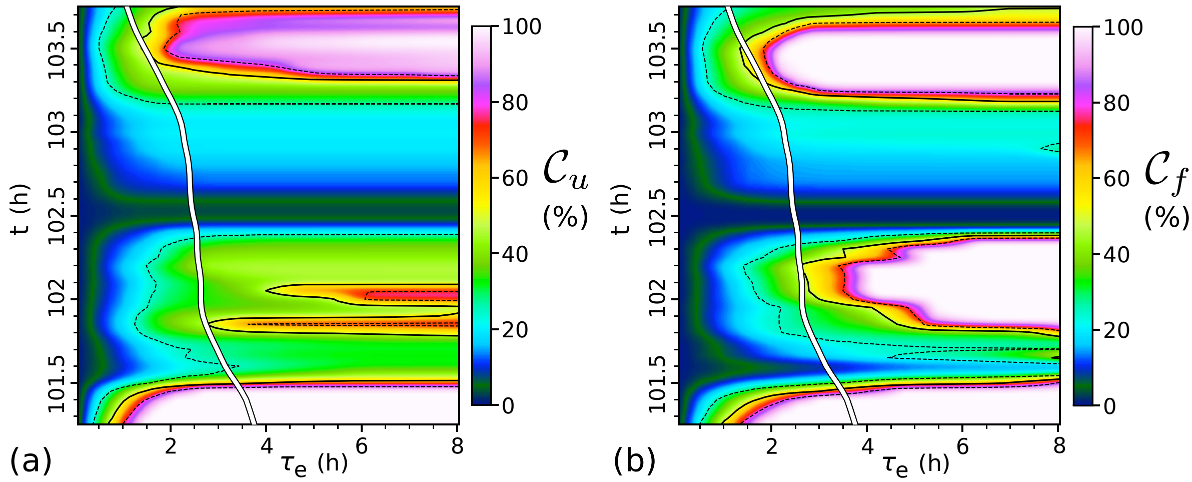

FIG. 10: Cumulative probability distributions for the escape time τ_e of a parcel randomly placed in the (a) unfiltered and (b) filtered CZ velocity field artificially frozen at time t, in the hours immediately preceding core reformation. The thick white line shows τ_{cr} for reference. The solid black curve shows the median of τ_e, whereas the dashed black curves show the 25th (left of the median) and 75th (right of the median) percentiles. Here it is assumed that $r_\sigma = 60$ km.

reformation and non-reformation scenarios will depend on the methodologies used to compute the time scales, and remains to be established through future research.

We remark in passing that the average ratio of the nominal entrainment radius r_o^{cr} (defined in section 2b) to $\lambda = \max(r_m, \ell)$ is less than 0.57 during the 2.5-h analysis period preceding t_{ref}, when calculated with $30 \leq r_\sigma \leq 60$ km. The corresponding average of τ_{cr} over τ_λ is less than 0.24. The proposed ancillary condition of r_o^{cr} falling well below λ (or τ_{cr} falling well below τ_λ) for CZ spinup to cause a virtually discontinuous change of the spatial parameters of the inner core (Fig. 4a) is thus firmly satisfied.

4d. Expanded Analysis

Before the CZ associated with core reformation emerges, the lower-tropospheric convergence field of the tropical cyclone is rather unsettled. Two or more CZs often coexist and switch their order of dominance over time. Furthermore, sporadic convection in the neighborhood of the dominant CZ sometimes causes its center (as measured herein) to abruptly shift. Whether a CZ loses its dominance or abruptly shifts, the change of $\mathbf{x}_\sigma$ over the corresponding sampling interval does not yield a sensible drift velocity. Nevertheless, the properties of CZs that dominate early on can be obtained during the periods between jumps of $\mathbf{x}_\sigma$. The following offers some evidence that these proper-

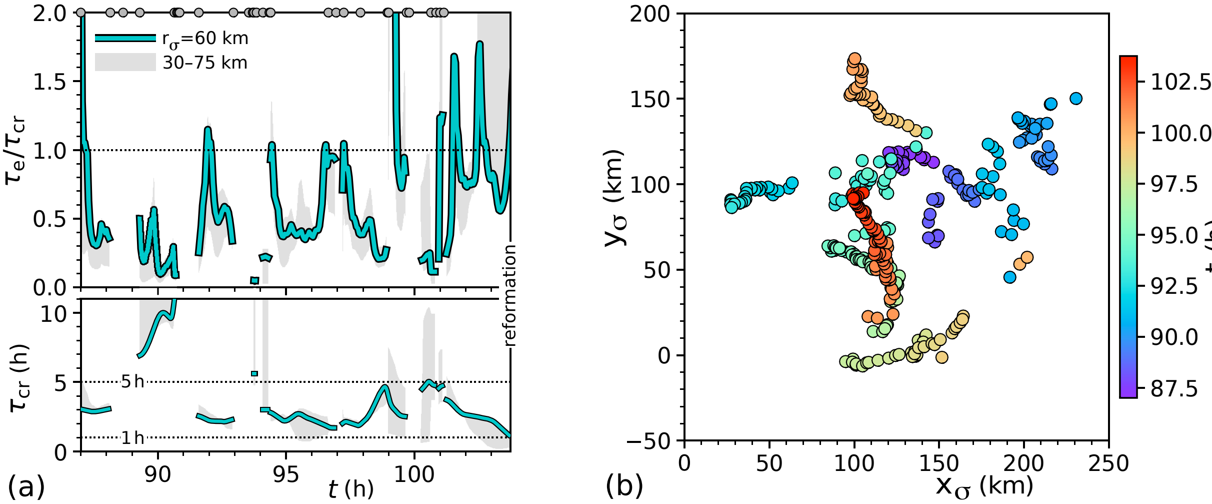

FIG. 11: (a) Expanded time series of τ_e/τ_{cr} (top) and τ_{cr} (bottom). The cyan curves in the top and bottom plots are obtained from Eqs. (11) and (6) with r_σ set to 60 km. The gray shading extends over the range of values (truncated at the upper limit of each plot) obtained with $r_\sigma \in \{30, 40, 50, 60, 75\}$ km. (b) Locations of the convergence center over the time period in (a) in a stationary coordinate system centered on the position of $\mathbf{x}_{cl}^b$ at t_{ref}.

ties are theoretically unsupportive of a reformation event over a range of plausible lengthscales including that of its eventual occurrence.

Figure 11a shows τ_{cr} and the ratio of τ_e [estimated by Eq. (11)] to τ_{cr} during the 17 hours prior to core reformation. The gray dots on the top axis coincide with the aforementioned jumps of $\mathbf{x}_\sigma$ (see Fig. 11b). The cyan curves are calculated assuming $r_\sigma = 60$ km so as to roughly match r_m of the reformed inner core at t_{ref}. Examination of the convergence field over the 17-h analysis period suggests that such an approximation usually results in the CZ containing the bulk of prominent positive anomalies near $\mathbf{x}_\sigma$. Note however that the fine structure of the convergence field within a 60-km radius of $\mathbf{x}_\sigma$ can differ from that seen shortly preceding reformation (Fig. 7) in having more pronounced negative anomalies alongside those of positive sign. Moreover, there are some intervals during which the strongest positive anomalies appear to lie beyond the 60-km radius, resulting in very small ($\ll 1$) values of τ_e/τ_{cr}. These intervals, which generally occur when the radius of maximum $\bar{u}_l^-$ (defined in section 3b) exceeds 90 km, have been removed from the time series. The gray shading that accompanies each cyan curve spans results for alternative values of r_σ (specified in the caption) between 30 and 75 km.

Consistent with theoretical expectations, the values of τ_e/τ_{cr} calculated for the dominant CZs (using any considered value of r_σ) tend to stay well below unity prior to the hours immediately before core reformation. Marginal exceptions are momentary and thus generally too short to create a new

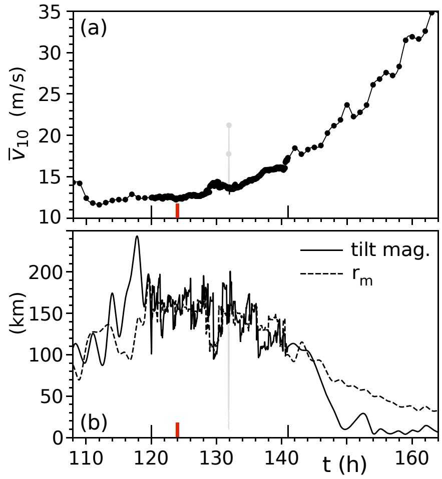

FIG. 12: (a) Time series of the maximum azimuthally averaged tangential velocity 10 m above the sea surface in a tropical cyclone simulation that does not exhibit core reformation during its principal phase of intensification. The time interval between consecutive data points is 3 min (1 h) in between (outside) the black ticks extending upward from the bottom axis. The red tick marks the approximate start of intensification. (b) Time series of the tilt magnitude (solid) and low-level radius of maximum wind speed r_m (dashed). The light gray glitch centered at t = 131.875 h results from an ignorable 10-km scale subvortex with fleeting (6-min) dominance.

inner core. The anomalous spike of the cyan curve just before the 100$^{\text{th}}$ hour of the simulation coincides with the production of a strong 10-km scale subvortex (mentioned at the end of section 4a) that quickly fades into subdominance.

Further comparison between the dynamics of a generic CZ that fails to induce core reformation and the exceptional CZ that succeeds would be instructive. Rather than choose an unsuccessful transient CZ from the present system, it was decided to choose one tracked over a much longer period of dominance in another tropical cyclone. The results are presented below.

5. The Failure of a Long-Lasting CZ to Induce Core Reformation

The following analysis pertains to a tropical cyclone simulated with an SST of 28 ^{o}C and an applied environmental vertical wind shear of 7.3 m s^{-1} measured from the surface to 12 km above sea level. This particular tropical cyclone begins a gradual asymmetric intensification process after roughly five days of development (Fig. 12a), at a time when the inner core is broad and strongly tilted. The intensification process shows no genuine sign of downtilt core reformation. Over the corresponding time period, the tilt magnitude and r_m (Fig. 12b) refrain from abruptly dropping in concert to permanently smaller scales as would be characteristic of such an event. Of further note, a single downtilt CZ dominates the convergence field during at least the first day of intensification. The central question at hand is whether the theory of section 2 can adequately explain why the dominant CZ fails to induce core reformation. Forthcoming analysis will provide a largely affirmative answer to this question after some preliminary matters are discussed.

5a. Setting of the Convergence Zone

The first matter to address is the setting of the dominant CZ. Figures 13 and 14 illustrate the state of the tropical cyclone at the onset of intensification. As before, the CZ is located in a region of heavy precipitation downtilt of the surface vortex center (Fig. 13). One notable difference between the present system and that considered previously (Fig. 5) is the lower mixed layer CAPE upstream of the CZ (Fig. 14a). The lower CAPE (related to the lower SST) is theoretically less conducive to vigorous deep convection, but does not seem prohibitive of core reformation based on the results of Rivera-Torres et al. (2023). Other differences that may exist are less apparent. As before, the CZ is centered slightly upstream of a near-surface cold pool (Fig. 14b) and contains high humidity supportive of deep convection (Fig. 14c). The low-level shear vectors (Fig. 14b) suggest substantial streamwise vorticity of air parcels entering the CZ. Relatively high values of BSH and SCP in the upstream vicinity of the CZ (Fig. 14d) give additional reason to believe that conditions are favorable for the maintenance of enhanced rotational convection. Subsequent snapshots (not shown) suggest that the CZ persists in a fairly similar setting for at least 17 hours into the future.

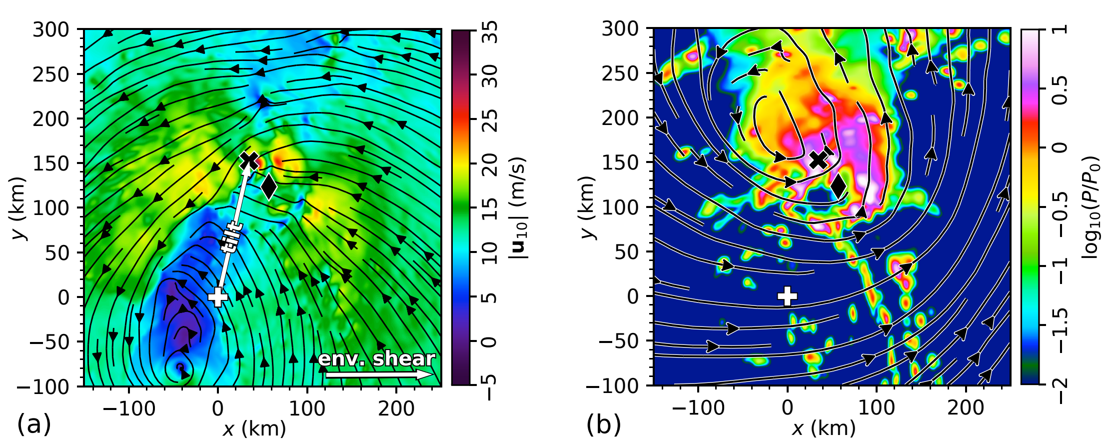

Fig. 13: (a) Snapshot of the streamlines and magnitude of the ground-relative surface velocity in a tropical cyclone simulated with moderate environmental vertical wind shear and a moderate SST, at the onset of an accelerated spinup process devoid of core reformation ($t = 124$ h). (b) Coinciding snapshot of the midlevel ($z \approx 8$ km) streamlines superimposed over the base-10 logarithm of the 6-min surface precipitation rate P normalized to $P_0 = 1$ cm h^{-1}. Symbols are as in Fig. 3.

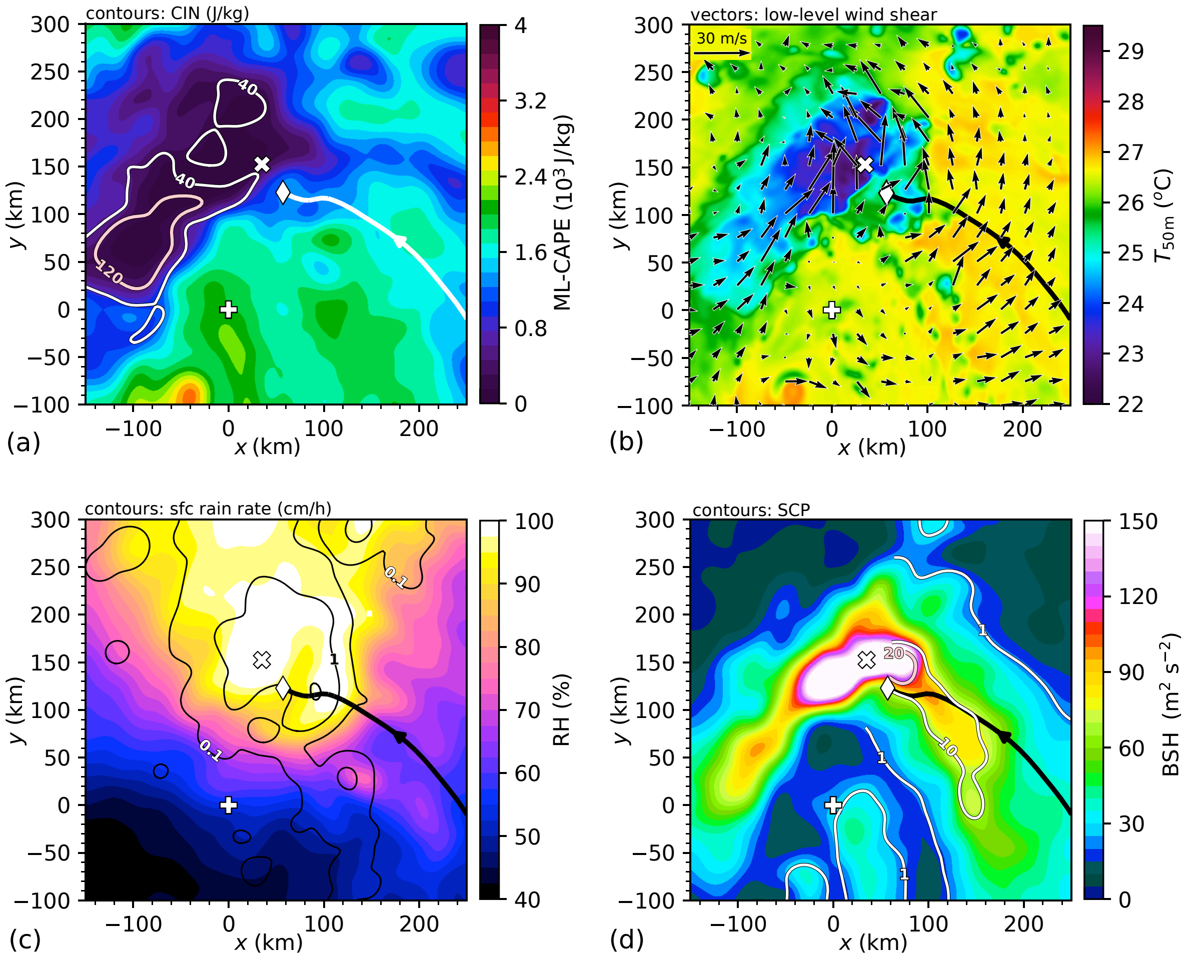

FIG. 14: Similar to Fig. 5 but for the tropical cyclone in Fig. 13 at t = 124 h, and with a minor adjustment to the near-surface temperature scale.

5b. Convergence Zone Dynamics

Figure 15 illustrates the CZ dynamics during a 1-h visualization period starting 30 min after the snapshot of section 5a. As in the left column of Fig. 7, the top row shows streamlines of the CZ-relative horizontal velocity field superimposed over the relative vorticity field in the boundary layer of the tropical cyclone. As in the middle column of Fig. 7, the bottom row shows streamlines of the filtered velocity field ($\mathbf{u}_f^*$) superimposed over the convergence field. The depicted 1-h evolution of the CZ begins with several prominent meso-γ scale clumps of positive vorticity within the 120-km wide dashed-gray circle that approximately bounds the CZ (Fig. 15a). Some of these clumps seem to have lost their prior connections to pronounced convergence anomalies (Fig. 15d) of the same scale. Moreover, neither the unfiltered (top) nor filtered (bottom) streamlines appear to show clear-cut points of attraction within the CZ. As a result of the foregoing conditions, the

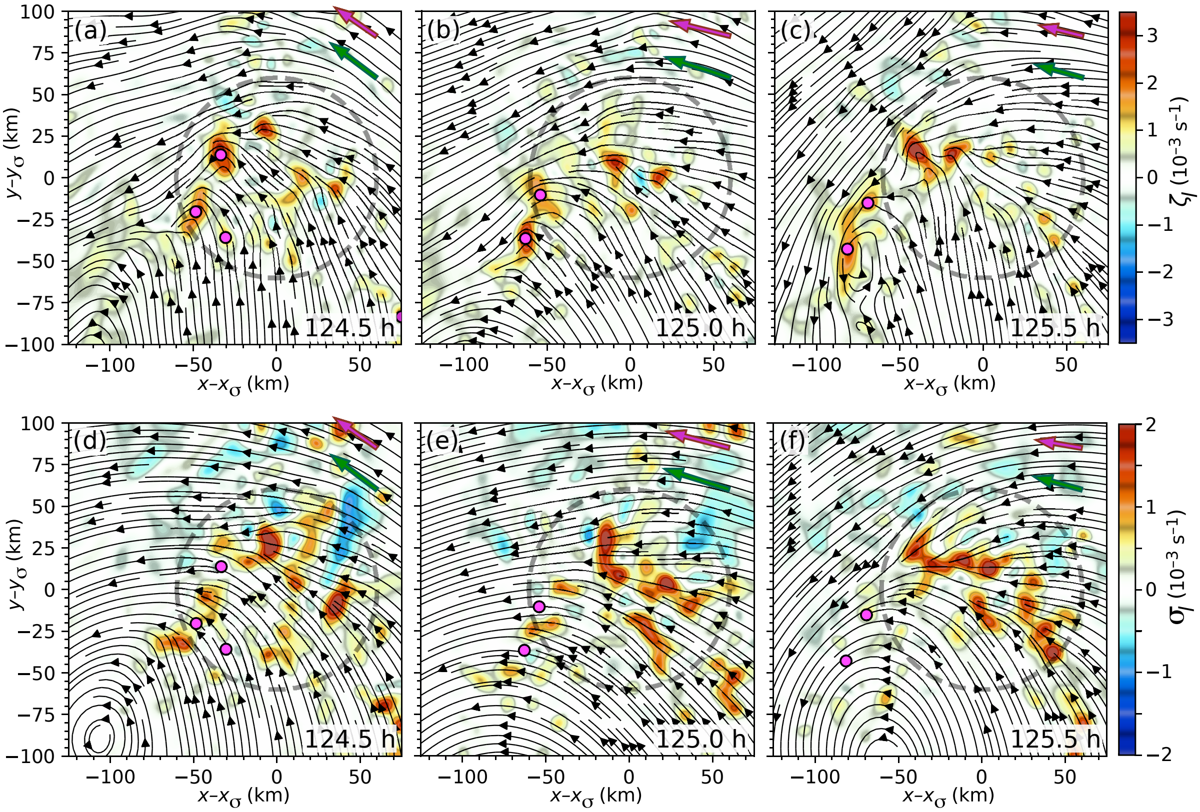

Fig. 15: (a-c) Snapshots of the boundary-layer relative vorticity field ζ_l (color) and streamlines of $\mathbf{u}_l^*$ during a selected 1-h segment of the evolution of a tropical cyclone as it begins to intensify without core reformation. (d-f) As in (a-c) but for the boundary-layer convergence field σ_l (color) and streamlines of $\mathbf{u}_f^*$. The dashed gray circle and colored vectors are as in Fig. 7, but with the magnitude of the green vector in (a) equaling 20.0 m s^{-1}. Purple dots track selected vorticity clumps. (The two clumps marked by the right-most dots at $t = 124.5$ h merge into the single clump marked by the upper-right dot at $t = 125$ h before exiting the CZ by $t = 125.5$ h.)

enhanced vorticity clumps (such as those marked by purple dots) tend to partially fade and stream out of the CZ into other parts of the tropical cyclone.

Figure 16a shows the tangential velocity budget [Eq. (17)] at the peripheral radius of the CZ during a 21-h analysis period starting just before the tropical cyclone begins a phase of accelerated intensification. As in Fig. 8, the tangential velocity budget is constructed in a reference frame that moves with the slowly drifting CZ (Fig. 16b), all terms are vertically averaged over the 1-km deep boundary layer, and the peripheral radius r_σ is estimated to be 60 km. The preceding estimate of r_σ is consistent with Fig. 15 and appears to be reasonable throughout the analysis period. In sharp contrast to the state of affairs during the lead-up to core reformation in Fig. 8, here the influx of absolute vorticity driven by the mean-flow (red curve) faces comparable opposition

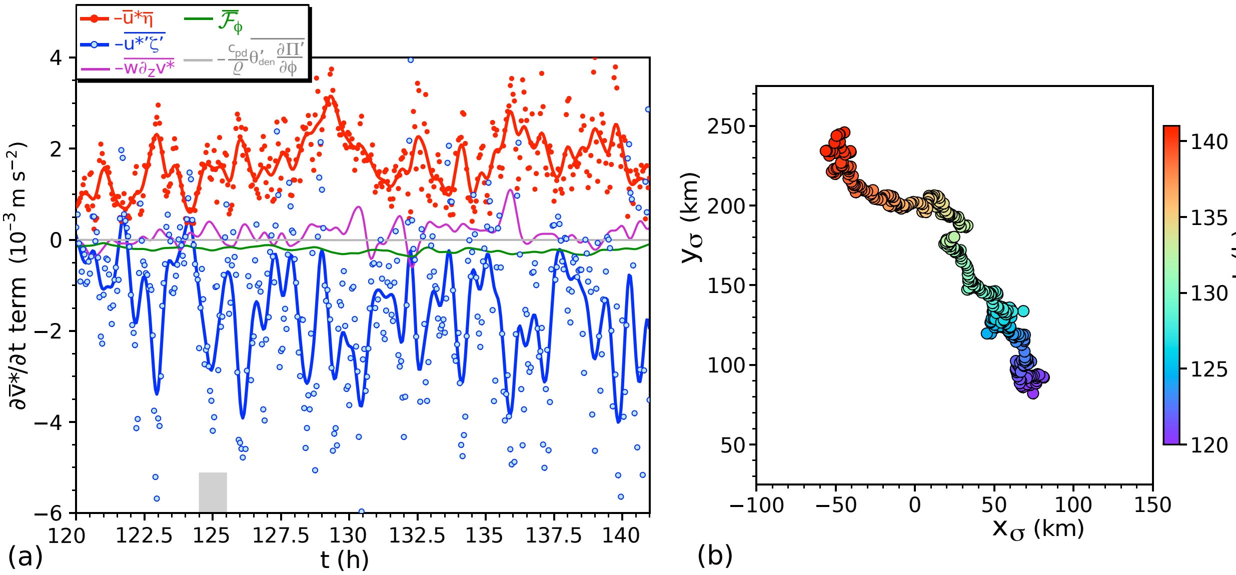

FIG. 16: (a) Contributions to the azimuthal velocity tendency [right-hand side of Eq. (17)] along the periphery of the dominant CZ of a tropical cyclone that fails to undergo core reformation, during a 21-h analysis period covering the early stage of intensification. All solid curves show time series that are Gaussian smoothed with a standard deviation parameter of 9 min to facilitate viewing; small red and blue circles show unsmoothed data for $-\overline{u^*\bar{\eta}}$ and $-\overline{u^{*\prime}\zeta^\prime}$, respectively. The width of the gray box on the bottom axis spans the time period of Fig. 15. (b) Trajectory of the CZ over the 21-h analysis period in a stationary coordinate system centered on the position of $\mathbf{x}_{cl}^b$ at $t = 124$ h.

from an eddy-driven outflux (blue curve) that acts to hinder local spinup. Expulsion of enhanced vorticity clumps by the background flow (as in Fig. 15) presumably contributes to the detrimental eddy-driven outflux.

We shall now address whether the dynamics hindering CZ spinup illustrated above actually coincides with a small ratio of the escape time to the unimpeded reformation time. The escape time τ_e is provisionally obtained without considering structural details of the CZ, and thus from Eq. (11) using the CZ-mean convergence for σ (as for evaluating τ_{cr}). Figure 17a shows that the corresponding simple estimate of τ_e/τ_{cr} tends to stay well below unity when calculated with r_σ between 30 and 75 km, and is therefore generally consistent with theoretical expectations for a CZ that is unsupportive of core reformation. On the other hand, a marginal anomaly ($\tau_e/\tau_{cr} \approx 1$) occurs in the vicinity of $t = 129$ h alongside a transient boost of the intensification rate (cf. Fig. 12a) for some of the assumed values of r_σ. Although short, the duration of this anomaly (roughly 1 h) is commensurate with the coinciding time scale τ_{cr} of unimpeded core reformation. What distinguishes the marginally conducive period for CZ spinup seen here from one that results in core reformation is uncertain, but could be related to neglected details of the CZ. If so, a probability

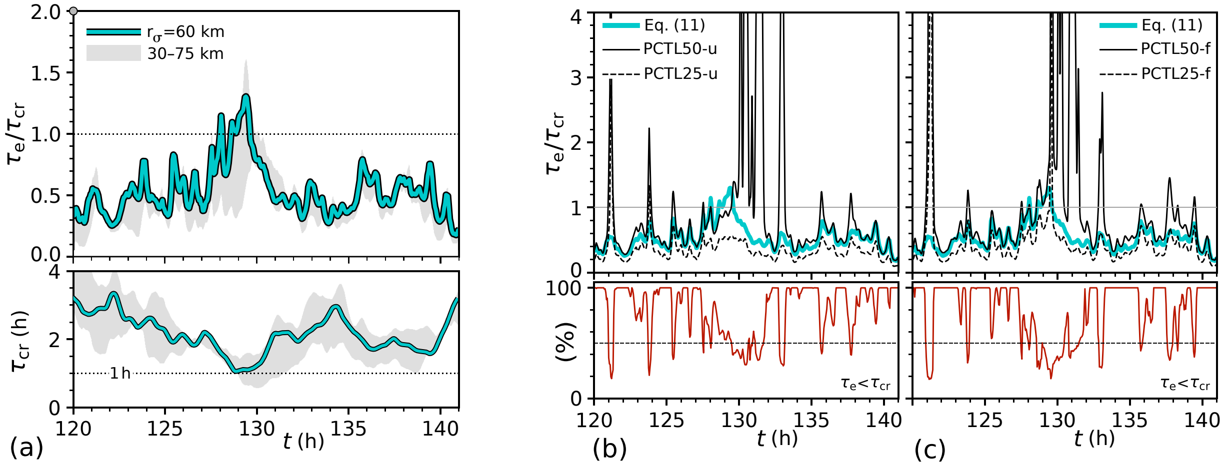

FIG. 17: (a, top) Time series of the ratio of τ_e [Eq. (11)] to τ_{cr} [Eq. (6)] over a 21-h analysis period during which a long-lasting CZ fails to induce core reformation as the encompassing tropical cyclone intensifies. The cyan curve and gray shading are as in Fig. 11. (a, bottom) Corresponding time series of τ_{cr}. (b, top) Time series of τ_e/τ_{cr} assuming $r_\sigma = 60$ km, calculated with (cyan) Eq. (11) for τ_e, (solid black) the 50$^{\text{th}}$ percentile of τ_e according to $\mathcal{P}_u$, and (dashed black) the 25$^{\text{th}}$ percentile of τ_e according to $\mathcal{P}_u$. (b, bottom) The probability for $\tau_e < \tau_{cr}$ given by the value of C_u at $\tau_e = \tau_{cr}$. The dashed black 50% line is drawn for reference. (c) As in (b) but with $\mathcal{P}_f$ and C_f replacing $\mathcal{P}_u$ and C_u.

distribution for τ_e ($\mathcal{P}_u$ or $\mathcal{P}_f$) accounting for such details may have a distinct feature indicating sufficient resistance to reformation.

Figures 17b and 17c compare the simple estimate of τ_e/τ_{cr} considered above to its 25$^{\text{th}}$ and 50$^{\text{th}}$ percentiles using the probability distribution $\mathcal{P}_u$ (left) or $\mathcal{P}_f$ (right) for τ_e assuming $r_\sigma = 60$ km [as in section 4 (Fig. 10) so that the sampling area of initial parcel positions covers the most prominent convergence anomalies near $\mathbf{x}_\sigma$ without excessive overextension]. Since the probability of an escape time smaller than τ_{cr} usually exceeds 50% (bottom panels), the 25$^{\text{th}}$ and 50$^{\text{th}}$ percentiles of τ_e/τ_{cr} usually fall below unity. Spikes of either percentile peaking above unity early and late in the time series seem too brief for relevance to core reformation. The moderately extended central cluster of spikes in the 50$^{\text{th}}$ percentile would appear to indicate favorable conditions for the CZ to generate a new inner core. However, the coinciding values of the 25$^{\text{th}}$ percentile from $\mathcal{P}_u$ (and but for an instant from $\mathcal{P}_f$) are well below unity. This stands in contrast to the immediate prelude of core reformation in the warm-ocean system of section 4, during which the 25$^{\text{th}}$ percentile distinctly spends roughly 1 h (one-half of τ_{cr}) far above unity (cf. Fig. 10). The implication that an appreciable fraction (albeit less than half) of the constituent fluid can escape the CZ through horizontal advection in a time less than τ_{cr} does not manifestly prohibit core reformation, but may well lower the chances of such an event.

6. Additional Instances of Core Reformation in the S24 Data Set

A critical reader may question whether the theoretically expected maintenance of τ_e near and above τ_{cr} during the hours preceding the simulated core reformation event of section 4 (Fig. 9a) is accidental. This concern can be addressed to some extent by investigating additional reformation events in the S24 data set. However, clear-cut instances of core reformation do not abound in the constituent simulations. Although strong 10-km scale subvortices occasionally emerge from the CZs of the tropical cyclones, they usually lose their momentary dominance to the original inner cores. One can also find a number of quasi-reformation events during which the center of the inner core shifts toward that of the CZ while r_m substantially contracts over a seemingly brief— but insufficiently short —advective time scale (roughly) given by the distance of the shift divided by the maximum wind speed. After eliminating provisional instances of core reformation with the preceding disqualifications, the author could still find a few cases to examine in addition to that of section 4. One such case entailed an appreciable discontinuity of $\mathbf{x}_\sigma$ moments before $t_{\rm cr}$ that prevented proper CZ diagnostics in the prelude of core reformation. Substantial parametrical adjustments of the rudimentary $\mathbf{x}_\sigma$ tracking algorithm (section 3b) were of no avail in removing the discontinuity. As explained below, the remaining two cases seem to be reasonably consistent with the basic theoretical ideas of section 2.[9]

The first additional case of core reformation entails a tropical cyclone simulated with an SST of 32 ^{o}C and a moderate environmental vertical wind shear of 9.8 m s^{-1} (from the surface to z = 12 km) that substantially misaligns the vortex before ramping down to zero at t = 87 h. Figure 18a shows that in this case, the tilt magnitude, r_m and ℓ discontinuously drop, rise and drop again between values of order 100 and 10 km over the time interval between 99.05 and 101.65 h. The first trough of the foregoing cycle coincides with the transient dominance of a 10-km scale subvortex inside the downtilt CZ. The first discontinuous drop and trough notably disappear in a reanalysis (not shown) that resets r_c to 30 km when searching for $\mathbf{x}_{cl}$, thereby ignoring the possibility of a viable inner core with a smaller radial lengthscale (see section 3b). Given its quick

[9] An objective algorithm for reliably identifying core reformation from the archived hourly simulation output was not developed for this study. Consequently, the author may have missed some of the reformation events that occurred in the S24 simulations. Those events apparent to the author from the time series of hourly sampled tropical cyclone parameters were resimulated to obtain the high-frequency (3-min) output required for thorough analysis.

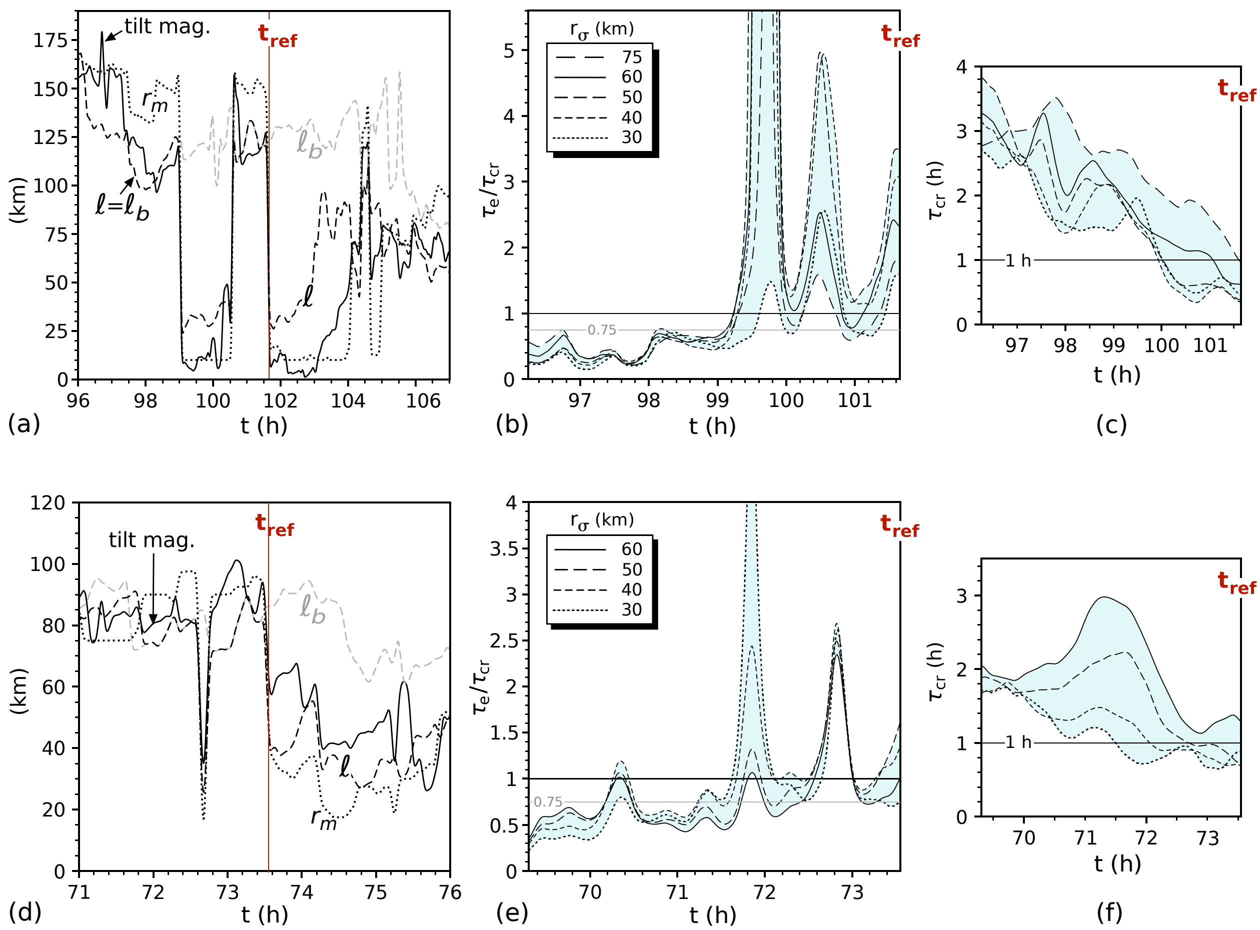

FIG. 18: (a-c) Synopsis of core reformation after the environmental vertical wind shear subsides in a simulation of a tropical cyclone over a relatively warm ocean. (a) Time series of pertinent tropical cyclone parameters (as in Fig. 4a). (b) Time series of the ratio of τ_e [Eq. (11)] over τ_{cr} [Eq. (6)] with r_σ given by the values in the legend (as in Fig. 9a). (c) Time series of τ_{cr} as in Fig. 9b. (d-f) As in (a-c) but for the tropical cyclone simulation of section 5 with a cooler ocean, well before the previously examined principal phase of intensification.

reversal and fragility, the first drop will not be viewed as the moment of core reformation. By contrast, the second discontinuous drop does not fully reverse and is maintained (with slight delay and smaller magnitude) even when adjusting r_c up to 70 km. Based on such robustness, the second drop is judged to mark the genuine moment of core reformation. It should be remarked that $\bar{v}_{10}$ is approximately 15 m s^{-1} at this time.

Figure 18b shows how the ratio of τ_e [Eq. (11)] to τ_{cr} [Eq. (6)] varies over the time period during which the CZ supporting core reformation was tracked prior to t_{ref}. Note that during the aforementioned transient dominance of a 10-km scale subvortex occurring between $t = 99.05$

and 100.55 h, the value of τ_{cr} is calculated with v_{mo} determined by the wind profile of the actual 100-km scale inner core. Consistent with theoretical expectations, the reformation event follows the elevation of τ_e/τ_{cr} to levels near and above unity for a time scale comparable to the mean of τ_{cr} (Fig. 18c). The preceding result appears to be valid using any r_σ within a range of values (30–75 km) deemed reasonable by inspection of the convergence field in the vicinity of $\mathbf{x}_\sigma$.

The second additional case of core reformation coincides with modest spinup of the surface vortex from depression to minimal storm intensity during an early evolutionary period of the tropical cyclone of section 5. The reformation event is marked by discontinuous drops of the tilt magnitude, r_m and ℓ at $t_{\text{ref}} = 73.55$ h to a range of values that remain relatively small for a substantial length of time (Fig. 18d). As before, the event follows a precursory moment (at $t = 72.65$ h) during which a 10-km scale subvortex dominates the true inner core. Again consistent with theoretical expectations, the official instant of core reformation immediately follows a distinct time period comparable to τ_{cr} (roughly two hours) during which the ratio of τ_e to τ_{cr} maintains levels near and above unity, assuming reasonable values of r_σ for this particular event between 30 and 50 km (Figs. 18e and 18f).[10] Note that after reformation, the moderate environmental vertical wind shear restores the misalignment of the tropical cyclone, and the low-level inner core gradually regresses into the broader weakened state seen before its primary phase of intensification (Fig. 12).

7. Summary

This paper has examined the circumstances under which a low-level convergence zone (CZ) associated with persistent downshear or downtilt convection may induce core reformation within a tropical cyclone. Basic theoretical considerations suggested that core reformation requires maintenance of the condition $\tau_{cr} < \tau_e$ over a time scale of order τ_{cr}. Here, τ_{cr} is an estimate [obtained from Eq. (6)] of the time scale of core reformation that neglects the disruptive impact of vorticity expulsion from the CZ by the nondivergent background flow, and τ_e is an estimate [Eq. (11)] of the time scale for fluid parcels to horizontally escape the CZ. In general, τ_{cr} decreases with increasing convergence or with increasing absolute vorticity surrounding the CZ. Sensibly, τ_{cr} also decreases toward zero as the mean tangential velocity along the periphery of the CZ increases toward the maximum wind speed of the tropical cyclone. The magnitude of τ_e distinctly grows

[10]The analysis with r_σ set to 60 km is shown for comparison to other cases, but may be inappropriately large in the present scenario.

from a finite minimum toward infinity as the convergence increases from zero toward a critical value σ_c [Eq. (10)]. The critical convergence σ_c notably decreases toward zero as the drift velocity of the CZ tends toward the local vector-value of the nondivergent background velocity field.

The simple condition for core reformation articulated above was tested against a small number of full-physics cloud resolving simulations of relatively weak and large tropical cyclones. Two of these simulations were examined in detail. In each of the detailed case studies, the primary analysis defined the CZ to have a radius (r_σ) of 60 km, so as to enclose the most prominent convergence anomalies near its center ($\mathbf{x}_\sigma$) without excessive overextension. The results (from sections 4 and 5) summarized below pertain to the primary analyses except where stated otherwise.

In the first case study (section 4) core reformation initiated a sustained period of fast spinup that transformed a weak tropical storm into a hurricane. Well before the reformation event, various CZs with transient dominance generally showed values of τ_e well below τ_{cr}. Brief blips of τ_e/τ_{cr} up to unity were evidently too short to have consequence. At a later time when τ_{cr} averaged around 2.4 h, the ratio of τ_e to τ_{cr} averaged closer to unity and had excursions markedly above unity. Consistent with slightly relaxed theoretical expectations, core reformation occurred within hours. Repeating the analysis with r_σ reduced to 40 or 30 km resulted in a more prominent rise of τ_e/τ_{cr} above unity in the hour preceding the reformation event. A speculative explanation for such improved conformity with the hypothesized reformation condition was offered in section 4c.

In the second case study of a tropical cyclone over a cooler ocean (section 5) the primary intensification process did not involve core reformation. A single CZ dominated a 21-h analysis period starting when the tropical cyclone transitioned to a phase of moderately paced spinup. Consistent with the theoretical condition hindering core reformation, the ratio τ_e/τ_{cr} remained well below unity with only a momentary marginal exception.

The presumption that small τ_e relative to τ_{cr} facilitates expulsion of enhanced vorticity from the CZ sufficiently fast to hinder core reformation was critically examined. Prompt expulsion was confirmed by sequential snapshots of CZ-enhanced vorticity anomalies during a typical period of the second case study with τ_e/τ_{cr} averaging about 0.5. Examination of the azimuthal velocity budget around the periphery of the CZ furthermore verified an eddy-outflux of vorticity effectively countering the local spinup tendency driven by the mean convergence of the CZ. By contrast, snapshots during the hours preceding core reformation in the first case study showed no indication of substantial vorticity expulsion from the CZ. In fact, the peripheral azimuthal velocity budget showed a measurable eddy-influx of vorticity contributing to CZ spinup. Note however that a negative eddy contribution to CZ spinup need not stifle core reformation if the positive influence of mean convergence dominates.

Alternative estimates of τ_e attempting to account for details of the CZ [neglected by Eq. (11)] were considered. Time-dependent probability distributions ($\mathcal{P}_f$ and $\mathcal{P}_u$) were constructed for the escape times of fluid parcels advecting along the artificially frozen streamlines of CZ-relative velocity fields with limited or no filtering. The limited filtering (used to obtain $\mathcal{P}_f$) retained details associated with the fine structure of the local convergence field but eliminated contributions from subcyclone scale vorticity anomalies. Replacing the simple estimate of τ_e with the first quartile of either distribution maintained a prominent excursion of τ_e above τ_{cr} shortly before core reformation occurred in the tropical cyclone of section 4. A similar replacement (especially when using $\mathcal{P}_u$) distinctly eliminated a marginal excursion of τ_e above τ_{cr} that occurred over a time scale comparable to τ_{cr} in the tropical cyclone of section 5 during an evolutionary period that failed to exhibit core reformation. The foregoing result hints that structural details of the CZ may hold the key to the success or failure of core reformation when the simplified estimate yields $\tau_e \approx \tau_{cr}$.

The S24 data set mined for this study did not contain an abundance of clear-cut core reformation events. Nevertheless, the author was able to find two extra events amenable to analysis (section 6). Both events were found to be consistent with that of section 4 in showing elevations of τ_e/τ_{cr} to levels near and above unity in the hours before the emergence of a new core. Thus, both events were essentially consistent with the hypothesized reformation condition.

It is worth reiterating (see section 2b) that the condition $\tau_{cr} < \tau_e$ at a given instant cannot alone predict imminent core reformation. Such a prediction would also require assurance that local convection will maintain an adequate combination of strength and drift-velocity to continuously support the preceding condition for a time scale of order τ_{cr}. Establishing a method to assess the probability of τ_e remaining above τ_{cr} from limited observations of regional meteorological conditions was viewed as beyond the scope of this study. One should also bear in mind that the condition required for CZ spinup ($\tau_{cr} < \tau_e$) may not guarantee a virtually discontinuous change of the inner core, which helps distinguish a reformation event from other pathways of evolution. An ancillary criterion for such abruptness of the transformation was put forth in section 2b.

In conclusion, this study has offered some insight into a competition between the convergent enhancement and horizontal expulsion of local vorticity that may largely determine whether core reformation will occur within the area of a low-level CZ. Moreover, this study appears to have made meaningful progress toward quantifying the condition for convergence to prevail. Subsequent studies will be required to fully elucidate what governs the strength of the CZ and the deviation of its drift velocity from the velocity of the background flow, which in theory partly regulates the expulsion of vorticity. Such studies might also aim to improve current understanding of how structural details of the CZ can affect the escape time τ_e.

Acknowledgments: The author duly thanks three anonymous reviewers for their constructive comments on the original version of this paper. The author also thanks Dr. George Bryan of the National Center for Atmospheric Research (NCAR) for developing and maintaining the atmospheric model used for this study (CM1). The simulations in the data set used for this study were made possible with resources provided by NCAR's Computational and Information Systems Laboratory (doi:10.5065/D6RX99HX). This work was supported by the National Science Foundation under Grant AGS-2208205.

Data Availability: CM1 parameter files and restart files (containing all prognostic atmospheric fields at various times during each CZ analysis period) will be available at https://doi.org/10.5281/zenodo.15701848 upon publication of this manuscript. Archived simulation output files too large and numerous for public repositories will be available to researchers upon request sent to schecter@nwra.com.

Appendix A: Appropriateness of Neglecting Friction

The derivation of the time scale of core reformation (t_{cr} or τ_{cr}) in section 2a is based on an axisymmetric model that neglects the negative influence of surface drag on the material derivative of the azimuthal velocity v. In an axisymmetric slab boundary layer of height h, the material derivative of v accounting for surface drag (controlled by the coefficient C_d) is given by

$$\frac{Dv}{Dt} = -\frac{uv}{r} - uf - \frac{\alpha^2 C_d |\mathbf{u}| v}{h}, \tag{A1}$$

in which α is the ratio of surface to boundary layer velocities. One can readily see that the frictional (last) term on the right-hand side of Eq. (A1) is negligible provided that

$$u(v + fr) \gg \alpha^2 C_d |\mathbf{u}| v \frac{r}{h}. \tag{A2}$$

Note that r should be interpreted as a radial lengthscale relevant to CZ spinup, which may extend up to $r_\sigma\sqrt{1+\sigma\tau_{cr}}$ in the model of section 2a. Condition (A2) basically implies that convection occurring in the CZ is coupled to an enhancement of radial inflow *far beyond* the point where the acceleration of v associated with angular momentum conservation balances the dissipation rate associated with surface drag.

In a more realistic system where the CZ is displaced from the vortex center, the equation governing the azimuthal mean of v (in a CZ-centered coordinate system) is complicated by nominal eddy contributions to the inertial and frictional terms. Fortunately, there is no present need for a comprehensive discussion of the circumstances under which the complexly modified frictional term is negligible. The precisely calculated CZ-centric azimuthal velocity budgets in Figs. 8 and 16a of this paper indicate that the total frictional forcing $\overline{\mathcal{F}}_\phi$ is subdominant in the primary case studies considered herein. While not shown in the aforementioned figures, this subdominance has been verified out to at least 100 km from the CZ center. Since $\overline{\mathcal{F}}_\phi$ accounts for both vertical and horizontal turbulent angular momentum transport, its smallness suggests that both surface friction and horizontal eddy viscosity are secondary to the essential dynamics of CZ spinup in the tropical cyclones at hand.

It should be noted that the preceding discussion of CZ spinup cannot be extended to the intensification of the broader cyclone, which is "forced" on its larger scale by a weaker inflow. The smaller inflow velocity at large r is ordinarily inconsistent with ignoring surface drag on the right-hand side of Eq. (A1). However, the only aspect of the large scale dynamics of relevance to calculating t_{cr} is the time dependence of the maximum tangential wind speed of the broader cyclone. The aforementioned wind speed usually varies slowly compared to the intrinsic pace of CZ spinup whether or not surface drag is incorporated into the model; such slowness is integral to the rationale behind approximating t_{cr} with τ_{cr} in practice. So, neglecting surface drag at all lengthscales for the virtue of simplicity (in a theory that is inherently limited to the natural time scale of CZ spinup) would seem to remain reasonable.

Appendix B: Outer Decay of the CZ-Centric Inflow Velocity

The formula used to estimate the time scale τ_{cr} of core reformation [Eq. (6)] assumes that the mean radial velocity $\overline{u}(\varrho)$ [in a polar coordinate system (ϱ,ϕ) centered on $\mathbf{x}_\sigma$] is inversely proportional to ϱ beyond the edge radius r_σ of the CZ, at least to the radius r_o^{cr} where the mean absolute angular momentum equals $r_\sigma v_{mo} + f r_\sigma^2/2$. For this to be true, the variable $\varrho\bar{u}$ should remain constant as the radius ϱ increases from r_σ to r_o^{cr}.

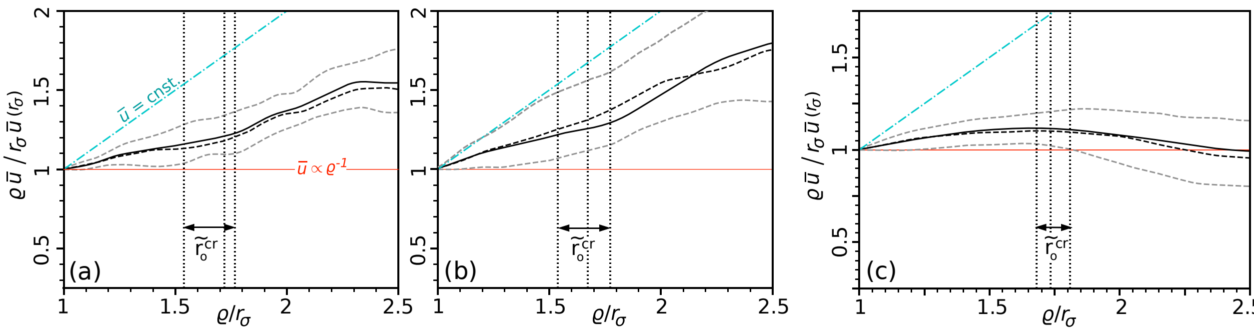

FIG. B1: (a) Plot of $\varrho\bar{u}$ normalized to its value at $r_\sigma = 60$ km versus ϱ/r_σ during the 2.5 hours prior to core reformation in the warm-ocean simulation of section 4. The solid (dashed) black curve is the mean (median) profile obtained from a set of snapshots taken every 3 minutes. The dashed gray curves show the first and third quartiles of normalized $\varrho\bar{u}$ at each ϱ. The red horizontal line corresponds to $\bar{u} \propto \varrho^{-1}$. Curves falling below the cyan dash-dotted line (corresponding to constant $\bar{u}$) indicate radial decay of the inflow velocity. The dotted vertical lines show the first, second and third quartiles of $\tilde{r}_o^{cr} \equiv r_o^{cr}/r_\sigma$. (b) As in (a) but for the 16.75 hours preceding $t_{\rm ref}$. (c) As in (a) but for $120 \le t \le 141$ h in the simulation with a moderate SST described in section 5.

Figure B1 illustrates the actual behavior of $\varrho\bar{u}$ normalized to its time-dependent value at r_σ (here assumed to be 60 km) during the primary scenarios examined for this study. Figure B1a corresponds to a 2.5-h examination of the area surrounding the dominant CZ immediately before the time $t_{\rm ref}$ of core reformation in the warm-ocean tropical cyclone simulation of section 4. Figure B1b is for the same simulation, but incorporates data from regions around multiple CZs during the 17 hours preceding $t_{\rm ref}$. Figure B1c represents 21 hours of data from the area surrounding a single CZ that fails to induce core reformation in the simulation with a moderate SST described in section 5.

Each panel of the figure reveals minor to moderate growth of $\varrho\bar{u}$ as ϱ increases from r_σ to r_o^{cr}. Such growth suggests that a better approximation of the outer radial velocity field in the domain of interest might be of the form $u_\kappa = -0.5\sigma r_\sigma^2[1+\kappa(\varrho - r_\sigma)]/\varrho$. The fractional error in using $\kappa = 0$ to estimate τ_{cr} is essentially given by $(\tau_0 - \tau_\kappa)/\tau_0$, in which τ_κ (τ_0) is the time for a parcel to travel from r_o^{cr} to r_σ for nonzero (zero) κ. For pertinent nonzero values of κ given by $\{0.1, 0.2, \ldots 0.5, 1.0\}/(r_o^{cr} - r_\sigma)$ with $r_o^{cr} = 1.75 r_\sigma$, the fractional errors are $\{0.05, 0.10, \ldots 0.20, 0.33\}$. These values are deemed sufficiently small to justify the $\kappa = 0$ approximation.

Appendix C: Reference Tables

This appendix contains several reference tables provided in compliance with an editorial request. Table C1 shows some general notational conventions used for coordinates and fluid fields. Table C2 shows various symbols introduced in sections 2a and 2b while deriving a testable condition for core reformation. Table C3 shows additional symbols used in subsequent sections for analyzing core reformation in the cloud resolving simulations.

Notation	Meaning
$\mathbf{x}$	horizontal position vector
x, y	Cartesian coordinates representing (left) eastward and (right) northward displacements from an arbitrary origin
z	height above the sea-surface
r, φ	(left) radius and (right) azimuth of a vortex-centered polar coordinate system
ϱ, ϕ	(left) radius and (right) azimuth of a CZ-centered polar coordinate system; same as r, φ for axisymmetric systems
t	time
$\mathbf{u}$	ground-relative horizontal velocity vector
u, v	ground-relative (left) radial and (right) azimuthal velocity around a specified pole, such as the tropical cyclone center or CZ center depending on context
w	vertical velocity
ζ, f, η	(left) relative, (middle) planetary and (right) absolute vertical vorticity
$*$	superscript used to indicate that a velocity (e.g. $\mathbf{u}^*$) is that observed in a CZ-relative reference frame
$\overline{\text{field}}$	azimuthal mean of a simulated fluid field around a specified pole
field′	perturbation of a simulated fluid field from its azimuthal mean (primes are occasionally used for other purposes)
~	accent used to denote a normalized variable as explained in section 2a
^	accent used to denote a unit vector
bold, non-bold	(left) vector and (right) scalar or component of a vector

TABLE C1. Some general notational conventions.

Symbol	Description	Remarks
τ_{cr}	estimated time scale for unimpeded (natural) core reformation	given by Eq. (6), interpreted for non-axisymmetric systems as explained in section 2b
τ_e	estimated time scale for fluid to horizontally escape the CZ	given by Eq. (11) or by a specified percentile derived from $\mathcal{P}_f$ or $\mathcal{P}_u$
σ	mean value of the low-level convergence field inside the CZ	———
σ_c	theoretical critical value of σ above which fluid cannot horizontally escape the CZ under a number of simplifying assumptions	defined by Eq. (10)
r_σ	radius (half-width) of the CZ	———
r_m	time-dependent (sections 4–6) or initial (section 2a) radius of maximum azimuthal velocity measured from the center of the low-level inner core of the tropical cyclone	———
v_o	initial azimuthally averaged low-level tangential velocity profile around the center of the CZ	for simulation analysis, "initial" refers to the time at which τ_{cr} and τ_e are estimated
v_{mo}	initial maximum azimuthally averaged low-level tangential velocity around the center of the inner core of the tropical cyclone	for simulation analysis, "initial" is interpreted as for v_o
ζ_o	initial relative vorticity distribution of the idealized axisymmetric system of section 2a	———
$2\Omega_o$	magnitude of the base component of ζ_o that extends to r_m	———
$\varepsilon \times (2\Omega_o r_m / r_\sigma)$	magnitude of the (additive) enhancement of ζ_o within the CZ	———
u_σ	radial velocity field attributable to the mean convergence σ inside the CZ in a CZ-centered coordinate system	———
r_o	initial radius of a contracting fluid ring in the axisymmetric vortex	given by Eq. (5) as a function of the current radius at an arbitrary time
t_{cr}	exact time required for core reformation in the idealized axisymmetric system of section 2a	ignores the possibility of turbulent stirring and radial variation of the convergence within the CZ
$\mathbf{u}_{\mathrm{cyc}}, \mathbf{u}_{\mathrm{env}}$	ground-relative horizontal velocity fields associated with (left) the broader cyclone containing the CZ and (right) the synoptic scale environmental winds	———
$\mathbf{c}_\sigma$	ground-relative translational velocity of the convergence center in a non-axisymmetric system	———
$\mathbf{u}_o^*$	approximation of the initial CZ-relative horizontal velocity field in the vicinity of a CZ in a non-axisymmetric system	sum of a local background flow and the convergent flow associated with the CZ
$\mathbf{U}_{\mathrm{bg}}, \mathbf{U}_{\mathrm{bg}}^*$	spatially invariant approximations of the (left) ground-relative and (right) CZ-relative background velocity field inside the CZ	———
ϱ_p	time-dependent radial distance traveled by a fluid parcel initially located at the center of an idealized CZ	———
r_o^{cr}	initial radius from the CZ center where the mean absolute angular momentum equals that required at r_σ for a mean tangential velocity of v_{mo}	———
λ	the greater of the initial value of r_m and the initial distance between the centers of the CZ and the inner core of the low-level vortex	———
τ_λ	the (hypothetical) time required for the radius of a fluid ring around the CZ center to contract from λ to r_σ assuming the inflow results solely from convergence inside the CZ	———

TABLE C2. Symbols pertaining to the basic theory of low-level core reformation in a tropical cyclone.

Symbol	Description	Remarks
$\mathbf{x}_{cl}$, $\mathbf{x}^{b}_{cl}$, $\mathbf{x}_{cu}$	position vectors for the centers of (left) the inner core of the low-level vortex, (middle) the low-level cyclonic circulation existing on a broader scale than the CZ and the reformed inner core, and (right) the midlevel vortex	measured as explained in section 3b
$\mathbf{x}_{\sigma}$, (x_{σ}, y_{σ})	(left) position vector for the center of the low-level CZ and (right) its Cartesian coordinates	measured as explained in section 3b
ℓ	distance between the low-level convergence and inner-core vortex centers	——-
ℓ_b	distance between the low-level convergence and broader cyclone centers	same as ℓ when the inner core is sufficiently broad
r_c	radius from a provisional vortex center below which winds are ignored when determining the associated maximum magnitude of $\bar{v}$ in the center-finding algorithm	see section 3b
t_{ref}	time at which core reformation occurs after the start of a simulation	——-
$\mathbf{u}_l$, $\mathbf{u}^*_l$	low-level horizontal velocity field in (left) ground-relative and (right) CZ-relative reference frames	obtained by vertical averaging over the lowest 1-km of the atmosphere
ζ_l, σ_l	low-level (left) relative vertical vorticity and (right) horizontal convergence fields	——-
v_l, v^*_l	(left) ground-relative and (right) CZ-relative low-level tangential velocity around a specified pole	——-
$\bar{u}^-_l$	minus-one times the low-level azimuthally averaged radial velocity around a specified pole	generally positive when taken around the CZ center
$\bar{v}_b$	low-level azimuthally averaged tangential velocity in a polar coordinate system centered at $\mathbf{x}^b_{cl}$	——-
$\bar{v}_{10}$	maximum $\mathbf{x}_{cl}$-centered azimuthally averaged tangential velocity of the tropical cyclone measured 10 m above the sea-surface	——-
$\mathbf{u}_a$	horizontal domain-average of $\mathbf{u}_l$	——-
$\mathbf{u}_{\chi}$	low-level horizontal velocity field attributable to convergence in the vicinity of the CZ	horizontal gradient of χ, in which χ is a solution to Eq. (14)
$\mathbf{u}_{\text{bg}}$, $\mathbf{u}^*_{\text{bg}}$	low-level background velocity field in (left) ground-relative and (right) CZ-relative reference frames	given by Eq. (16) in the ground-relative reference frame
$\mathbf{u}^*_f$	filtered low-level horizontal velocity field in the CZ-relative reference frame	defined by Eq. (13)
$\mathcal{P}_f$, C_f	(left) probability distribution (right) cumulative probability distribution for the time required by a parcel to escape the CZ along the artificially frozen streamlines of $\mathbf{u}^*_f$	see section 2c and Eq. (18)
$\mathcal{P}_u$, C_u	(left) probability distribution (right) cumulative probability distribution for the time required by a parcel to escape the CZ along the artificially frozen streamlines of $\mathbf{u}^*_l$	see section 2c and Eq. (18)
Π	Exner function (dimensionless pressure variable)	——-
θ_{den}	density potential temperature	——-
$\mathcal{F}_{\phi}$	acceleration of azimuthal velocity around the CZ center attributable to parameterized turbulent momentum transport	——-

TABLE C3. Additional symbols used for simulation analysis.

References

Alvey III, G.R., M. Fischer, P. Reasor, J. Zawislak, and R. Rogers, 2022: Observed processes underlying the favorable vortex repositioning early in the development of Hurricane Dorian (2019). *Mon. Wea. Rev.*, **150**, 193-213.

Alvey III, G.R. and A. Hazelton, 2022: How do weak, misaligned tropical cyclones evolve toward alignment? A multi-case study using the Hurricane Analysis and Forecast System. *J. Geophys. Res.: Atmospheres*, **127**, e2022JD037268:1-27.

Bryan, G.H., and J.M. Fritsch, 2002: A benchmark simulation for moist nonhydrostatic numerical models. *J. Atmos. Sci.*, **130**, 2917-2928.

Bryan, G. and R. Rotunno, 2009: The maximum intensity of tropical cyclones in axisymmetric numerical model simulations. *Mon, Wea. Rev.*, **137**, 1770-1789.

Bunkers, M.J., B.A. Klimowski, J.W. Zeitler, R.L. Thompson, and M.L. Weisman, 2000: Predicting supercell motion using a new hodograph technique. *Wea. Forecasting*, **15**, 61-79.

Chen, X., Y. Wang, J. Fang, and M. Xue, 2018: A numerical study on rapid intensification of Typhoon Vicente (2012) in the South China Sea. Part II: Roles of inner-core processes. *J. Atmos. Sci.*, **75**, 235-255.

Chou, M.-D., and M. Suarez, 1999. A Solar Radiation Parameterization for Atmospheric Studies. *NASA Tech. Memo.* 104606, **15**, 38 pp.

Chou, M.D., M.J. Suarez, X.Z. Liang, and M.M.H. Yan, 2001: A thermal infrared radiation parameterization for atmospheric studies. *NASA Tech. Memo.* 104606, **19**, 68 pp.

Curcic, M. and B.K. Haus, 2020. Revised estimates of ocean surface drag in strong winds. *Geophys. Res. Lett.*, **47**, e2020GL087647:1-8.

Davis, C.A., S.C. Jones, and M. Riemer, 2008: Hurricane vortex dynamics during Atlantic extratropical transition. *J. Atmos. Sci.*, **65**, 714-736.

Drennan, W.M., J.A. Zhang, J.R. French, C. McCormick, and P.G. Black, 2007: Turbulent fluxes in the hurricane boundary layer. Part II: Latent heat flux. *J. Atmos. Sci.*, **64**, 1103-1115.

Dunion, J.P., 2011: Rewriting the climatology of the tropical North Atlantic and Caribbean Sea atmosphere. *J. Climate*, **24**, 893-908.

Fairall, C.W., E.F. Bradley, J.E. Hare, A.A. Grachev, and J.B. Edson, 2003: Bulk parameterization of air-sea fluxes: Updates and verification for the COARE algorithm. *J. Climate*, **16**, 571-591.

Hendricks, E.A., M.T. Montgomery and C.A. Davis, 2004: The role of "vortical" hot towers in the formation of Tropical Cyclone Diana. *J. Atmos. Sci.*, **61**, 1209-1232.

Houze Jr., R.A., 2010: Clouds in tropical cyclones. *Mon. Wea. Rev.*, **138**, 293-344.

Judt, F., R. Rios-Berrios, and G.H. Bryan, 2023: Marathon versus sprint: two modes of tropical cyclone rapid intensification in a global convection-permitting simulation. *Mon. Wea. Rev.*, **151**, 2683-2699.

Kilroy, G. and R.K. Smith, 2015: Tropical cyclone convection: The effects of a vortex boundary-layer wind profile on deep convection. *Q. J. R. Meteorol. Soc.*, **141**, 714-726.

Molinari, J., D. Vollaro, and K.L. Corbosiero, 2004: Tropical cyclone formation in a sheared environment: A case study. *J. Atmos. Sci*, **61**, 2493-2509.

Molinari, J., P. Dodge, D. Vollaro, K.L. Corbosiero, and F. Marks, 2006: Mesoscale aspects of the downshear reformation of a tropical cyclone. *J. Atmos. Sci.*, **63**, 341-354.

Molinari, J., and D. Vollaro, 2010a: Rapid intensification of a sheared tropical storm. *Mon. Wea. Rev.*, **138**, 3869-3885.

Molinari, J., and D. Vollaro, 2010b: Distribution of helicity, CAPE, and shear in tropical cyclones. *J. Atmos. Sci.*, **67**, 274-284.

Morrison, H., J.A. Curry, and V.I. Khvorostyanov, 2005: A new double-moment microphysics parameterization for application in cloud and climate models. Part I: Description. *J. Atmos. Sci.*, **62**, 1665-1677.

Morrison, H., G. Thompson, and V. Tatarskii, 2009: Impact of cloud microphysics on the development of trailing stratiform precipitation in a simulated squall line: Comparison of one-and two-moment schemes. *Mon. Wea. Rev.*, **137**, 991-1007.

Nguyen, L.T., and J. Molinari, 2015: Simulation of the downshear reformation of a tropical cyclone. *J. Atmos. Sci.*, **72**, 4529-4551.

Rivera-Torres, N.G., K.L. Corbosiero, and B.H. Tang, 2023: Factors associated with the downshear reformation of tropical cyclones. *Mon. Wea. Rev.*, **151**, 2717-2737.

Rogers, R.F., P.D. Reasor, J.A. Zawislak, and L.T. Nguyen, 2020: Precipitation processes and vortex alignment during the intensification of a weak tropical cyclone in moderate vertical shear. *Mon. Wea. Rev.*, **148**, 1899-1929.

Rotunno, R. and J.B. Klemp, 1982: The influence of the shear-induced pressure gradient on thunderstorm motion. *Mon. Wea. Rev.*, **110**, 136-151.

Schecter, D.A., 2020: Distinct intensification pathways for a shallow-water vortex subjected to asymmetric "diabatic" forcing. *Dyn. Atmos. Oceans*, **91**, 101156:1-25.

Schecter, D.A., and K. Menelaou, 2020: Development of a misaligned tropical cyclone. *J. Atmos. Sci.*, **77**, 79-111.

Schecter, D.A., 2023: Intensification rates of tropical cyclone–like vortices in a model with downtilt diabatic forcing and oceanic surface drag. *J. Atmos. Sci.*, **80**, 1787-814.

Schecter, D.A., 2024: Two types of transitions to relatively fast spinup in tropical cyclone simulations with weak to moderate environmental vertical wind shear, *J. Atmos. Sci.*, **81**, 1513–1541.

Smith, R.K., and M.T. Montgomery, 2012: Observations of the convective environment in developing and non-developing tropical disturbances. *Q. J. R. Meteorol. Soc.* **138**, 1721-1739.

Stone, Ž., G.R. Alvey III, J.P. Dunion, M.S. Fischer, D.J. Raymond, R.F. Rogers, S. Sentić, and J. Zawislak, 2023: Thermodynamic contribution to vortex alignment and rapid intensification of Hurricane Sally (2020). *Mon. Wea. Rev.*, **151**, 931-951.

Thompson, R.L., R. Edwards, J.A. Hart, K.L. Elmore, and P. Markowski, 2003: Close proximity soundings within supercell environments obtained from the Rapid Update Cycle. *Wea. Forecasting*, **18**, 1243-1261.